A

MAJOR PROJECT REPORT

ON

A SURVEY ON UNDER WATER WIRELESS COMMUNICATION TECHNOLOGY

Submitted in partial fulfillment of the requirement for the award of degree of

BACHELOR OF TECHNOLOGY

IN

ELECTRONICS AND COMMUNICATION ENGINEERING

SUBMITTED BY

K. SAKETH	**218R1A04F8**
K. AJAY VARDHAN REDDY	**218R1A04F9**
K.KRUSHI	**218R1A04G0**
K.NAGA POOJITHA	**218R1A04G1**

Under the Esteemed Guidance of

Mrs.G.PRAVALIKA

Assistant Professor

DEPARTMENT OF ELECTRONICS & COMMUNICATION ENGINEERING

CMR ENGINEERING COLLEGE

UGC AUTONOMOUS

(Approved by AICTE, Affiliated to JNTU Hyderabad, Accredited by NBA)
Kandlakoya(V), Medchal(M), Telangana – 501401

(2024-2025)

CMR ENGINEERING COLLEGE

UGC AUTONOMOUS
(Approved by AICTE, Affiliated to JNTU Hyderabad,
Accreditedby NBA) Kandlakoya (V), Medchal Road,
Hyderabad - 501 401

DEPARTMENT OF ELECTRONICS AND COMMUNICATION ENGINEERING

CERTIFICATE

This is to certify that Major project work entitled **"A SURVEY ON UNDER WATER WIRELESS COMMUNICATION TECHNOLOGY"** is being Submitted by **K.SAKETH** bearing Roll No:**218R1A04F8, K.AJAY VARDHAN REDDY** bearing Roll No:**218R1A04F9, K.KRUSHI** bearing Roll No:**218R1A04G0, K.NAGA POOJITHA** bearing Roll No:**218R1A04G1** in B.Tech IV-II semester, Electronics and Communication Engineering is a record bonafide work carried out by then during the academic year 2024-25.

INTERNAL GUIDE:
Mrs .G.PRAVALIKA

HEAD OF THE DEPARTMENT
Dr. SUMAN MISHRA

EXTERNAL EXAMINER

ACKNOWLEDGEMENTS

We sincerely thank the management of our college **CMR Engineering College** for providing required facilities during our project work. We derive great pleasure in expressing our sincere gratitude to our Principal **Dr. A. S. Reddy** for his timely suggestions, which helped us to complete the project work successfully. It is the very auspicious moment we would like to express our gratitude to **Dr. SUMAN MISHRA**, Head of the Department, ECE for his consistent encouragement during the progress of this project.

We take it as a privilege to thank our project coordinator **Dr. T. SATYANARAYANA,** Associate Professor, Department of ECE for the ideas that led to complete the project work and we also thank him for his continuous guidance, support and unfailing patience, throughout the course of this work. We sincerely thank our project internal guide **Mrs.G.PRAVALIKA**, Associate Professor of ECE for guidance and encouragement in carrying out this project work.

DECLARATION

We hereby declare that the major project entitled **"A SURVEY ON UNDER WATER WIRELESS COMMUNICATION TECHNOLOGY"** is the work done by us in campus at **CMR ENGINEERING COLLEGE**, Kandlakoya during the academic year 2024-2025 and is submitted as major project in partial fulfilment of the requirements for the award of degree of **BACHELOR OF TECHNOLOGY** in **ELECTRONICS AND COMMUNICATION ENGINEERING FROM JAWAHARLAL NEHRU TECHNOLOGICAL UNIVERSITY, HYDERABAD.**

K. SAKETH	**(218R1A04F8)**
K. AJAY VARDHAN REDDY	**(218R1A04F9)**
K.KRUSHI	**(218R1A04G0)**
K.NAGA POOJITHA	**(218R1A04G1)**

CONTENTS

ABSTRACT

Underwater wireless communication (UWC) refers to the transmission of data in the underwater environment using optical, radio-frequency (RF), or acoustic waves. This thesis specifically focuses on UWC that employs optical waves as transmission carriers. Compared to RF and acoustic counterparts, UWC offers a significantly higher transmission bandwidth, enabling much higher data rates. This advantage has garnered substantial attention in recent years, with numerous potential applications for UWC systems proposed in areas such as environmental monitoring, offshore exploration, disaster management, and military operations. However, UWC systems face substantial challenges due to severe absorption and scattering effects in the underwater channel. To address these issues, several novel system design approaches, which differ from traditional terrestrial free-space optical communication systems, have been explored. In this thesis, we present a comprehensive survey of the state-of-the-art research in UWC across three critical areas: channel characterization, modulation and coding techniques, and practical system implementations. Based on a thorough understanding of UWC, we also investigate the outage performance of vertical buoy-based UWC systems in the presence of pointing errors. We derive the closed-form outage probability for systems with zero boresight pointing errors and provide outage probability bounds for nonzero boresight pointing errors, further advancing the understanding of the system's reliability and performance under practical conditions. Further, building on the comprehensive understanding of UWC systems, this thesis investigates the outage performance of vertical buoy-based UWC systems, particularly focusing on the impact of pointing errors that arise when aligning the optical communication link between the transmitter and receiver. Pointing errors, such as those caused by platform motion, environmental disturbances, or misalignment of optical devices, can significantly reduce the link reliability. To quantify this impact, we derive the closed-form outage probability for UWC systems assuming zero boresight pointing errors, providing a baseline for system performce.

LIST OF FIGURES

LIST OF TABLES

CHAPTER 1

INTRODUCTION

1.1 OVERVIEW OF THE PROJECT

Two thirds of the earth's surface is covered with water. During the past thousands of years, humans have never stopped the exploration of the ocean. In recent years, with an increase of globe climate change and resource depletion of land, there has been a growing interest in the researchof ocean exploration system. Underwater wireless communication (UWC) technology enables the realization of ocean exploration systems, and thus attracts more and more attention. UWC refers to transmitting data in an unguided water environment through the use of wireless carriers, i.e. radio-frequency (RF) waves, acoustic waves, and optical waves. Considering the limited bandwidth of RF and acoustic methods and the increasing need for high-speed underwater data transmission, Underwater Wireless Communication Technology (UWC) has become an attractive and viable alternative. In fact, light has been used as a wireless communication method for thousands of years in various forms.

For instance, the ancient Chinese used beacon towers in order to deliver military information around 1,000 BC, and the ancient Greek and Roman armies used polished shields to reflect sunlight for signaling around 800 BC. In 1880, Alexander Graham Bell developed a new wireless telephone system that used sunlight as the transmission medium. This system is regarded as the first optoelectronic communication system in the world 12, 13. In the 1960s, the invention of laser as an ideal optical source has changed the future of optical wireless communication (OWC) 14. From that time on, a flurry of terrestrial OWC applications appeared. But due to the severe attenuation effects of seawater to visible light and the limited knowledge of aquatic optics, the earlydevelopment of UWC was far behind the terrestrial free-space optical (FSO) communications.Based on nearly 20 years experimental and theoretical study of light propagation in the sea,in 1963, Duntley proposed that seawater shows a relatively low attenuation property to light with wavelengths from 450nm to 550nm which corresponds to the blue and green spectrum (Figure 1.1) 15. mainly for military purpose, especially in the area of submarine communications. In 1976, Karp evaluated the feasibility of wireless optical communications between underwater and above surface (satellite) terminals 17.

In 1977, the researchers in the Lawrence Livermore Laboratory of the University of California proposed an one- way optical communication system from shore to submarine 18. The transmitter of the UWC system employed blue-green laser source to generate light pulses. It was flexible to be carried by a land vehicle or an airplane due to its compact architecture. The transmitter can also focus its output light beam on a relay satellite, which then reflects the beam to a submarine 18. Other UWC tests of the plane-to-submarine and satellite-to-submarine topologies were established by US and Russian navy during 1980s and 1990s 19. Mixed optical communication links with about tens of kilometers FSO link and several tens of meters UWC link were achieved.

Over the decades, the interest of UWC is still limited to military applications 18, 20. The massive market promotion of UWC has not been achieved so far. Only a few limited UWC products were commercialized in the early 2000s, such as the BlueComm UWC system which can achieve 20 Mbps underwater data transmission over 200m distance, and the Ambalux UWC system which can provide the same data transmission rate in a shorter range of 20m 21. In order to satisfy the increasing demands for ocean exploration with efficient high bandwidth data transmission, researchers have proposed the concept of underwater wireless sensor networks (UWSNs).

The proposal of UWSNs has greatly facilitated the development of UWC. Thus the market of UWC has begun to show a future promise. The basic UWSNs consist of many distributed nodes such as seabed sensors, relay buoys, autonomous underwater vehicles (AUVs) and remotely operated underwater vehicles (ROVs) (Figure 1.2). These nodes have capabilities to accomplish sensing, processing, and communication tasks that maintain the collaborative monitoring to the underwater environment 4. In Figure 1.2, sensors located at the bottom of the seabed collect data and transmit via acoustic or optical links to the AUVs and ROVs. Then, AUVs and ROVs relay signals to ships, submarines, communication buoys and other underwater vehicles. Above the sea surface, the onshore data center processes data and communicates with satellite .

The range of wavelengths in which light penetrates water most effectively. This window lies primarily in the blue and green regions of the spectrum, as these wavelengths are least absorbed by water.

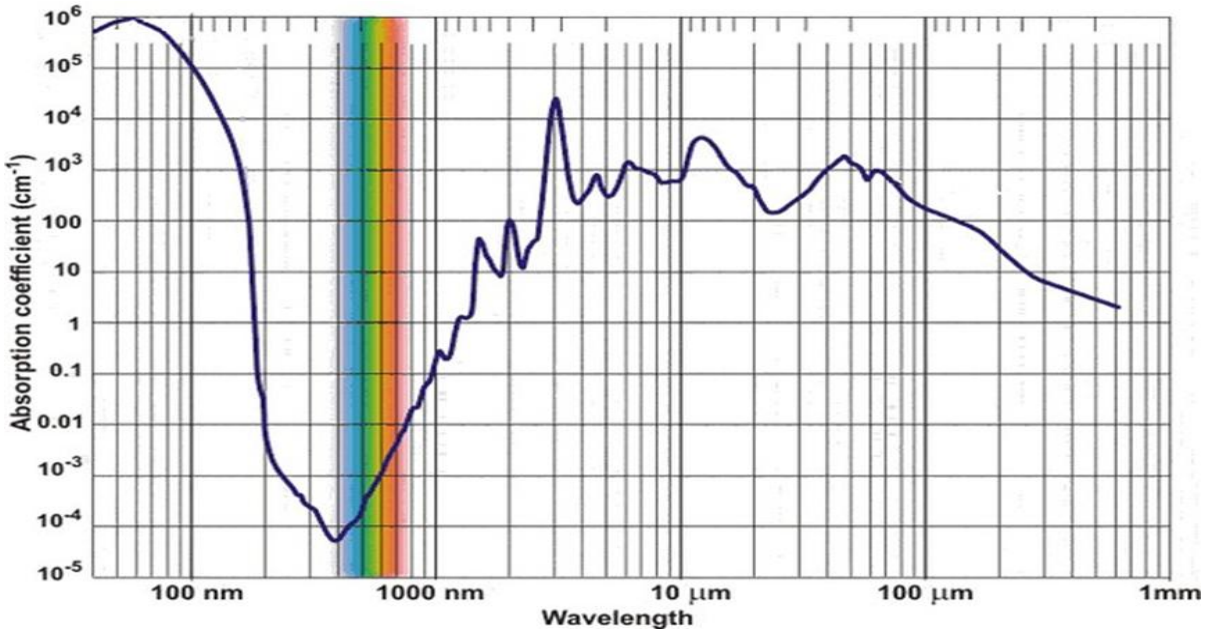

Figure 1.1 The transparent window for light aquatic attenuation is shown with blue and green colour

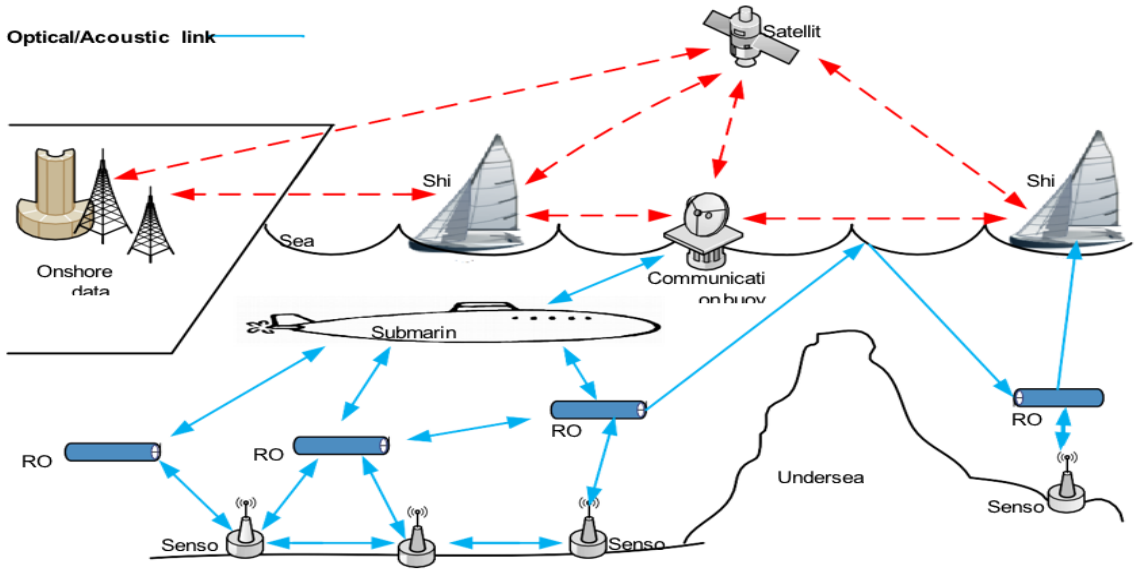

Figure 1.2: An Underwater Wireless Sensor Network With Aerospace and Terrestrial Communication.

Line-of-Sight (LOS) configuration refers to a direct, unobstructed path between a transmitter and receiver, essential for efficient signal transmission in many communication systems. It is particularly critical in optical and high-frequency radio systems, where obstacles can significantly degrade or block the signal. LOS ensures minimal signal loss, lower latency, and better overall link quality. In underwater optical communication, maintaining LOS is crucial due to high attenuation and scattering in water. Any misalignment or obstruction, such as marine life or floating debris, can disrupt the communication link..

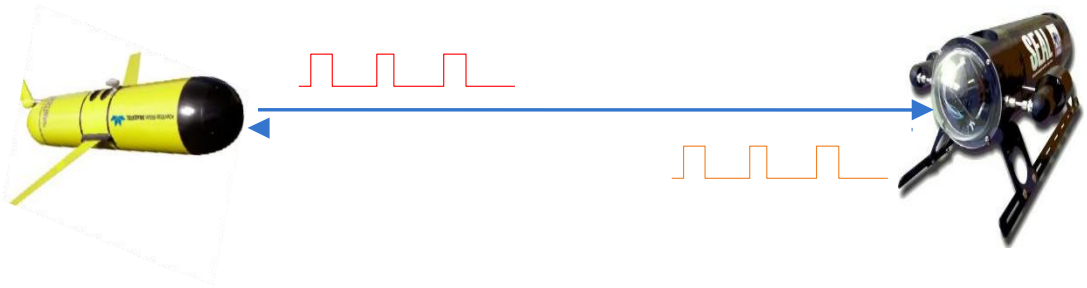

Figure 1.3 (a)Point-to-point LOS configuration.

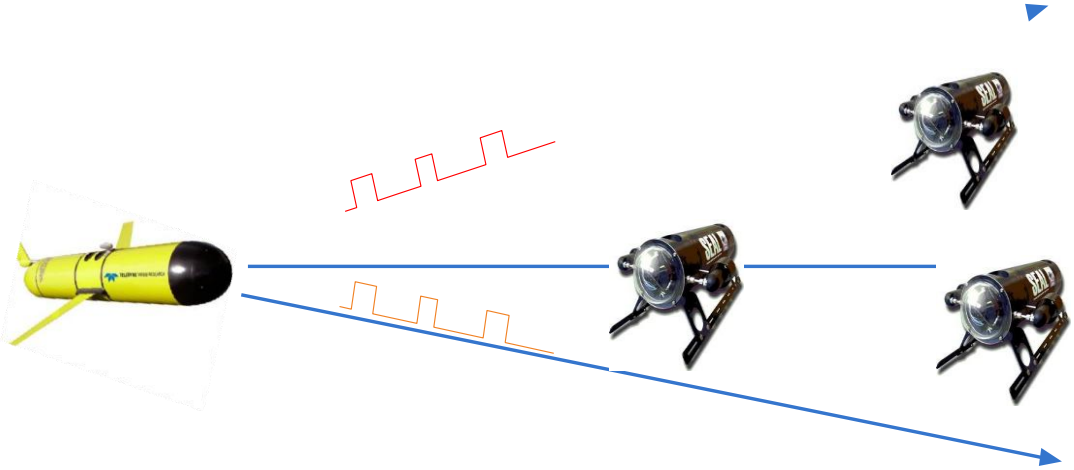

Figure 1.4 (b)Diffused LOS configuration.

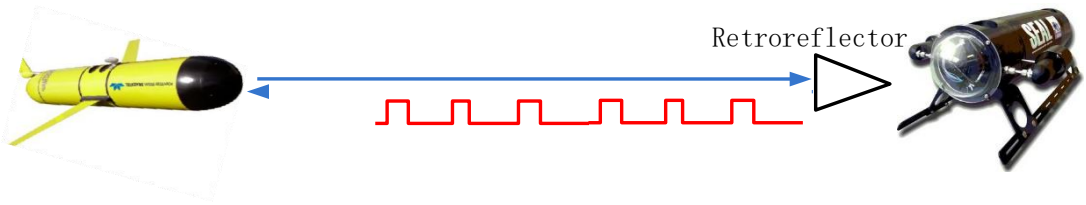

Figure 1.5 (c)Retroreflector-based LOS configuration.

1. Point-to-point LOS configuration (Figure 1.3(a)) is the most commonly used link configuration in UWC [23]. In point-to-point LOS configuration, the receiver detects the light beam in the direction of the transmitter. Since the point-to-point LOS UWC system commonly employs light sources with a narrow divergence angle, such as a laser, it requires precise pointing between transmitter and receiver. This requirement will limit the performance of UWC systems in turbid or turbulent water environments and then becomes a severe problem when the transmitter and the receiver are non-stationary nodes, such as AUVs and ROV [22].

2. Diffused LOS configuration employs diffused light sources with large divergence angle such as high-power light-emitting diodes (LEDs) to accomplish broadcasting UWC from one node to multiple nodes (Figure 1.3(b)). Broadcasting method can relax the requirement of precise pointing. However, compared with the point-to-point LOS configuration, the diffused-light based link suffers from aquatic attenuation due to the large interaction area with water. Relatively short communication distances and lower data rates are the two major limitations of this configuration.

3. Retroreflector-based LOS configuration, as shown in Figure 1.3(c), can be regarded as one special implementation of point-to-point LOS configuration. This configuration is suitable for duplex UWC systems having limited power and weight budget, such as an underwater sensor node. In modulating retro-reflector link, the transmitted light is reflected back from a modulated retro-reflector. During this process, the information that the retroreflector responses to the transceiver will be encoded on the reflected light. Since there is no laser or other light sources in the retroreflector end, its power consumption, volume and weight will be tremendously reduced. One limitation of this configuration is that the backscatter of the transmitted optical signal may interfere the reflected signal, thus degrading the system signal to noise ratio (SNR) and bit-error-rate (BER). Moreover, since the optical signals will go through the underwater channel twice, received signal will experience additional attenuation. . In underwater environment, matters such as chlorophyll are capable of absorbing the blue and red lights. These matters and other colored dissolved organ- ic material (CDOM) can increase the turbidity of the water, and thus shrink the propagation distance of the light.

1.2 ADVANTAGES AND CHALLENGES OF UWC

UWC systems are used for high speed underwater communications between multiple fixed or mobile nodes. They have great potential for applications in the UWSNs. Conventionally, there are three UWC choices for implementing UWSNs: acoustics, RF and optics 1. In order to emphasize the unique advantages and characterizations of UWC, we will compare the UWC with RF and acoustic methods in the following of this section.

The acoustic method is the most widely used technology in UWC. It has a long application history that can be dated to late 1800s. After an extensive expansion of military applications during the two World Wars, underwater acoustic communication system has become a popular proven technology that has been applied to almost every aspect of UWSNs 26. Considering the extreme broadness of ocean and the strong attenuation effect of seawater to other transmission sources like optical wave and RF wave, the most attractive advantage of underwater acoustic communication is that it can achieve a long link range up to several tens of kilometers Although acoustic method is the most popular method to achieve UWC, it also has certain intrinsic technical limitations. Firstly, since the typical frequencies associated with underwater acoustics are between 10 Hz and 1 MHz, the transmission data rate of acoustic link is relatively low (typically on the order of kbps) . Secondly, due to the slow propagation speed of sound wave in water (about 1500m/s for 20 Celsius pure water), the acoustic link suffers from severe communication delay (typically in seconds). Thus it can't support applications which require real-time large volume data exchange. Thirdly, acoustic transceivers are usually bulky, costly and energy consuming. They are not economical for large scale UWSNs implementations 28. Furthermore, acoustic technology can also impact marine life which uses sound waves in order to accomplish communication and navigation 29.

The underwater RF electromagnetic (EM) communication can be seen as an extension of the terrestrial RF-EM communication. The underwater RF communication has two major advantages. First, compared with acoustic wave and optical wave, the RF wave can perform a relatively smooth transition through air/water interface . This benefit can be used to achieve the cross-boundary communication which combines the terrestrial RF communication system and underwater RF-EM communication system together. Second, RF-EM method is more tolerant to water turbulence and turbidity than optical and acoustic methods .

The fatal limitation that impedes the development of underwater RF-EM method is its short link range. Since seawater that contains lots of salt is a conductive transmission media, the RF waves can only propagate a few meters at extra-low frequencies (30-300Hz) . Moreover, the underwater RF-EM systems also require huge transmission antenna and costly, energy-consuming transceivers.

Compared with the acoustic approach and RF-EM approach, UWC has the highest transmission data rate, lowest link delay and the lowest implementation costs. UWC can achieve a data rate on the order of Gbps over moderate distances of tens of meters. This high-speed advantage will guarantee the realization of many real-time applications such as underwater video transmission. Since the transmission speed of light in water is much higher than acoustic wave, UWC links are immune to link latency. UWC also has higher communication security over the acoustic and RF methods. Most UWC systems are implemented in LOS configuration, rather than the diffused broadcasting scenario like acoustic and RF wave. It becomes more difficult to be eavesdropped. Furthermore, UWC is much more energy efficient and cost-effective than its acoustic and RF counterparts. Instead of using large and expensive acoustic and RF transceivers which are highly energy consuming, relatively small and low-cost optical underwater transceivers, such as laser diodes and photo diodes, can be implemented in UWC systems. This benefit can improve the large scale commercialization of UWC, and accelerate the implementations of UWSNs.

Although UWC enjoys many advantages over the acoustic and RF methods, achieving UWC remains as a challenging task. The main challenges of UWC are listed as follows.

Optical signal suffers from severe absorption and scattering. Although the wavelength of transmission light has been carefully selected in the blue and green spectrum to minimize the transmission attenuation coefficient, due to the inevitable photon interactions with the water molecules and other particulate matters in water, absorption and scattering still severely attenuate the transmitted light signal and cause multi-path fading. Due to the impact of absorption and scattering, UWC suffers from poor BER performance over a few hundred meters link distance in turbid water environment. In underwater environment, matters such as chlorophyll are capable of absorbing the blue and red lights. These matters and other colored dissolved organic material (CDOM) can increase the turbidity of the water.

Implementation of UWC systems requires reliable underwater devices. The underwater environment is complex. The flow, pressure, temperature and salinity of seawater will strongly impact the performance light. Moreover, the concentration of CDOM will also change with ocean depth variations, thus change the corresponding light attenuation coefficients 30. These undesirable impacts will in.

Underwater optical links will be temporarily disconnected due to misalignment of optical transceivers.In several UWC systems, blue/green lasers or LEDs have been implemented as the lightsources due to their narrow divergence feature; however, a precise alignment condition is required. As the underwater environment is turbulent at relatively shallow depths, link misalignment will take place frequently, especially in the vertical buoy-based surface-to-bottom UWC applica- tions. Random movements of sea surface will cause serious and lifetime of UWC devices. Considering that no solar energy can be exploited undersea and the long undersea operation time of UWC devices, the reliability of device batteries and efficiency of device power consumption are critical.

CHAPTER 2

UWC Channel Modeling

In this chapter, we will firstly present background knowledge related to light propagation properties in the underwater environment. Then, UWC channel modeling techniques, which include link attenuation modeling, geometric misalignment modeling, and turbulence modeling, will be presented. Finally, we will summarize this chapter and organize the related literatures in one table.

2.1 LIGHT PROPAGATION IN WATER

Compared with terrestrial FSO communication channels, UWC channels have several unique characteristics. The existing terrestrial FSO channel models are not suitable for underwater environ- ment; therefore, new reliable channel models must be proposed and studied. In order to derive new channel models for UWC, we have to firstly understand the basic properties of light propagation in the underwater environment.

According to Mobley's statements in 5, the optical properties of water can be classified into two different groups: inherent optical properties (IOPs) and apparent optical properties (AOPs). IOPs can be understood as the optical parameters that only depend on the transmission medium itself, more specifically the composition of that medium and particulate substances present within it 22. They are independent of the characterizations of light sources. The major IOPs of water are the absorption coefficient, the scattering coefficient, the attenuation coefficient, and the volume scattering function 31. AOPs, on the other hand, are known as the optical parameters that depend not only on the the transmission medium itself, but also the geometrical structure of the light field such as diffusion and collimation 22. The three major AOPs of water are radiance, irradiance and reflectance 31. In a UWC system, IOPs are typically used determining communication link budgets, whereas AOPs are used to calculate ambient light levels for communication systems near the ocean surface 22. Since IOPs have a greater impact on the link performance. In the rest of this section, we will focus on IOPs. The details of AOPs that include their definitions and measurements can be found in 5.

Absorption and scattering coefficients are the two major IOPs that determine the underwater light attenuation. Absorption is an energy transfer process in which photons lose their energy and convert it into other forms, such as heat and chemical (photosynthesis). Scattering is caused by variations in the refractive index that changes the propagation direction of photons 35. Generally, the impacts of absorption and scattering to a UWC system can cause three undesirable effects. First, in the presence of absorption, the total propagation energy of light is continuously decreasing, which will limit the link distance of the UWC. Second, in the presence of scattering, since the size of optical aperture is finite, scattering will spread the light beam and result in a reduction of the number of photons collected by the receiver. This will lead to degradation of SNR of the system. Third, due to the light scattering in an underwater environment, each photon may arrive at the receiver panel in different time slots, and multi-path dispersions will occur. The undesirable impacts of multi-path phenomenon include inter symbol interference (ISI) and timing jitter.

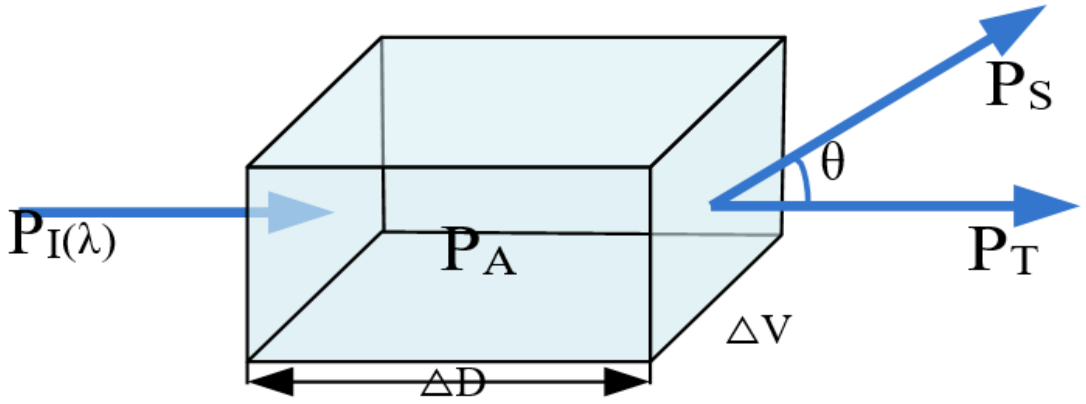

Figure 2.1: Geometry of inherent optical properties for a volume ΔV .

In order to derive the absorption and scattering coefficients mathematically, we introduce the simple model in Figure 2.1. We assume that a volume of water ΔV with thickness ΔD is illuminated by a collimated light beam with wavelength λ. We denote the power of incident light as P_I. A portion of the incident light power P_A is absorbed by water, and another portion of light power P_S[1] is scattered. P_T is the remaining light power that will propagate as desired. According to the lawof conservation, we get 5, 36 $P_I = P_A + P_S + P_T$. (2.1)

Sequent absorption coefficient and scattering coefficient are then calculated by taking the limit of absorbance and scatterance as water thickness ΔD becomes infinitesimally small 5, In underwater optics, the overall attenuation effects of absorption and scattering can be described by the attenuation coefficient [2] $c(\lambda)$ which can be expressed as 38.

The unit of attenuation coefficient is m^{-1}. In addition, the author of 2 states that the underwater light absorption coefficient can be further represented as the summation of four absorption factors where $a_w(\lambda)$ is the absorption due to pure seawater, $a_{CDOM}(\lambda)$ is the absorption due to CDOM, $a_{phy}(\lambda)$ denotes the absorption due to phytoplankton, and $a_{det}(\lambda)$ represents the absorption due to detritus.

The absorption effect of pure seawater is introduced from two sources: the water molecules and dissolved salt in water such as NaCl, $MgCl_2$, Na_2SO_4, and KCl 39. Pure seawater is absorptive except around a 400nm-500nm window, the blue-green region of the visible light spectrum. The corresponding absorption spectrum of pure seawater is shown in Figure 2.2(a).CDOM [3] refers to colored dissolved organic materials with dimensions smaller than 0.2 mm 40. In Figure 2.2(b), it shows that the CDOM presents highly absorptive to blue wavelengths (420nm-450nm) and less absorptive to yellow and red light 41.

The absorption effects due to phytoplankton are mainly caused by photosynthesising of chloro- phyll. For different phytoplankton species, the characteristics of the absorption effect different 42. Figure 2.2(c) shows a typical absorption coefficient profile shared by all species. We can observe that the $a_{phy}(\lambda)$ shows a high absorption in the 400-500 nm region and a further peak at about 660 nm.

Detritus includes living organic particles, such as bacteria, zooplankon, detrital organic matter and suspended inorganic particles such as quartz and clay. These substances are grouped together due to their similar absorption behaviour 43. Figure 2.2(d) shows a absorption curve similar to that if CDOM. The scattering coefficient for underwater light propagation can also be presented as a summation of different scattering factors where $b_w(\lambda)$ is the scattering due to pure seawater, $b_{phy}(\lambda)$ denotes the scattering due to phytoplank- ton, and $b_{det}(\lambda)$ represents the scattering due to detritus. Compared with absorption, scattering is relatively independent of wavelength. The dominant factor that impacts scattering is the density of particulate matters.

In pure seawater, since the refractive index will change with the variations of flow, salinity and temperature, the scattering coefficient will also change. Compared with the size of water molecules, the wavelength of light is relatively large, thus the Rayleigh scattering model can be used to describe the scattering induced by pure seawater. The corresponding scattering spectra is shown in Figure 2.3(a).

$$b(\lambda) = b_w(\lambda) + b_{phy}(\lambda) + b_{det}(\lambda)$$

Phytoplankton and detritus account for more than 40% of the total scattering effects 44. Since the scattering light caused by phytoplankton and detritus propagates mainly in the forward direc- tion, Mie scattering model can be used to approximate these two types of scattering 5. In practice, the exact scattering coefficients highly depends on the density of phytoplankton and detritus 45. In Figure 2.3(b) and Figure 2.3(c), we present the scattering spectra due to phytoplankton and detritus with different densities. A summary of the above discussion on seawater absorption and scattering characteristics is presented in Table 2.1

To model this kind of forward scattering, the Mie scattering model is often used. The Mie theory is a well-established approach for describing light scattering by spherical particles, and it is particularly useful for situations where the particle size is comparable to the wavelength of light. Phytoplankton, which are tiny plant-like organisms in the water, and detritus, which consists of decomposing organic material, both exhibit scattering properties that can be approximated by Mie scattering when their size distribution and optical properties are taken into account.

The Mie model can help to predict how light interacts with these particles in the ocean However, it is important to note that the exact scattering coefficients—parameters that quantify the intensity of scattered light—are not fixed but are highly dependent on the density of both phytoplankton and detritus. As the concentration of these particles in the water increases, the scattering of light becomes more pronounced, and the overall optical properties of the seawater change. This relationship underscores the variability of scattering effects in different aquatic environments, which can range from clear waters with low phytoplankton and detritus .

The optical absorption spectra for different ocean components show how various substances absorb light at different wavelengths. Pure water absorbs red and infrared light strongly, allowing blue and green light to penetrate deeper. Phytoplankton absorb mainly in the blue and red regions due to pigments like chlorophyll. Colored Dissolved Organic Matter (CDOM) absorbs strongly in the ultraviolet and blue regions. Suspended sediments can cause broadband absorption and scattering, affecting overall water clarity and color.

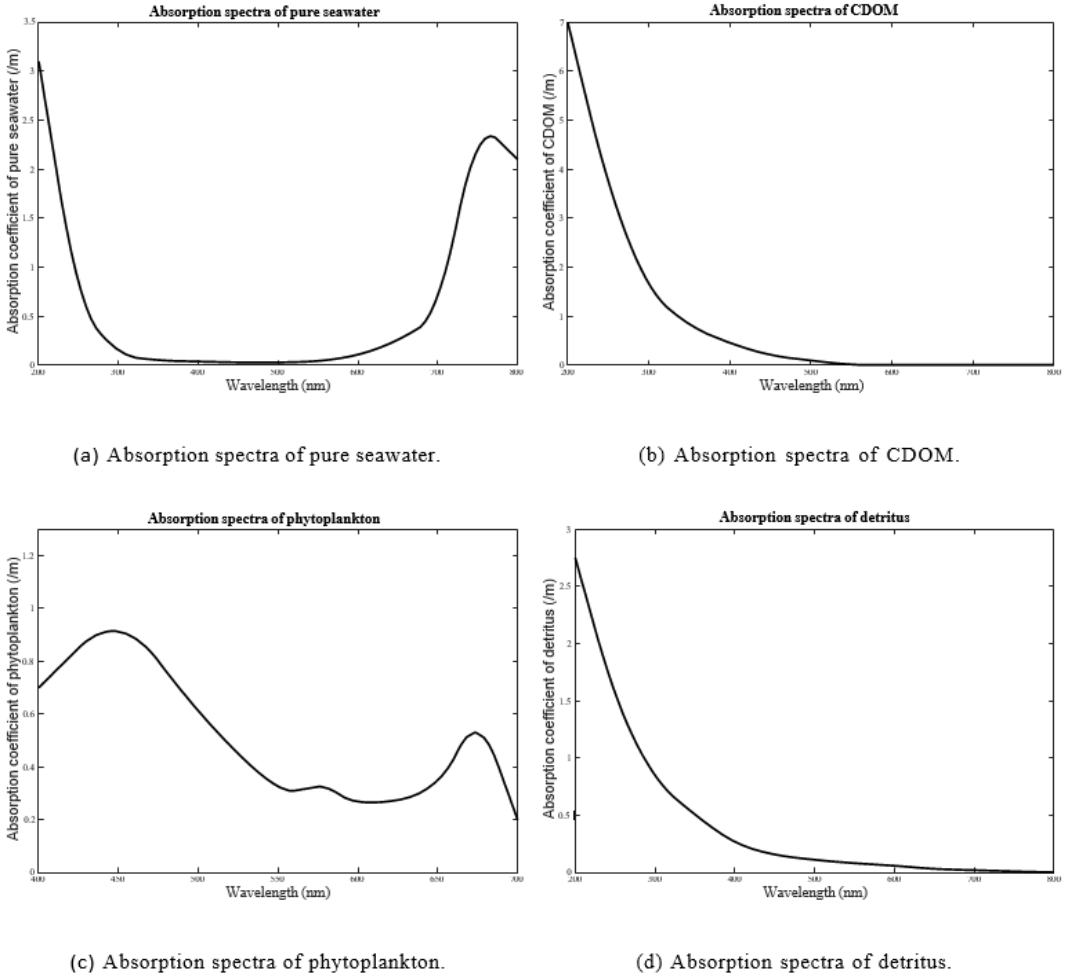

(a) Absorption spectra of pure seawater.

(b) Absorption spectra of CDOM.

(c) Absorption spectra of phytoplankton.

(d) Absorption spectra of detritus.

Figure 2.2: Optical Absorption Spectra For Different Ocean Components.

TThe optical scattering spectra for different ocean components explain how light is redirected in various directions by particles in seawater. Pure water causes minimal scattering, with blue light scattered more than red due to its shorter wavelength. Phytoplankton contribute to scattering depending on their size and structure, often enhancing scattering in the green region. Colored Dissolved Organic Matter (CDOM) has minimal scattering but can still affect light behavior indirectly. Suspended sediments, especially inorganic particles like silt or sand, produce strong and broad-range scattering. The size, shape, and concentration of these particles influence the intensity and direction of scattered light. Overall, scattering affects underwater visibility, remote sensing accuracy, and how light penetrates the ocean.

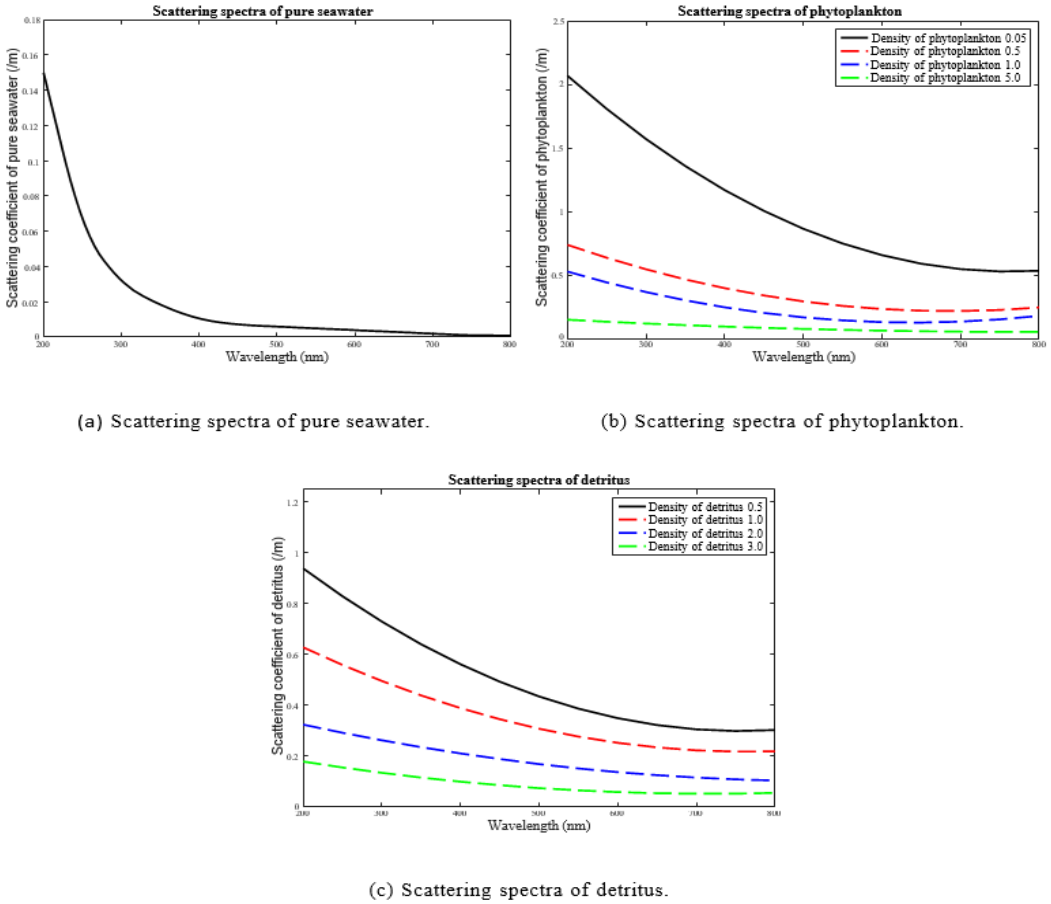

(a) Scattering spectra of pure seawater.

(b) Scattering spectra of phytoplankton.

(c) Scattering spectra of detritus.

Figure 2.3: Optical Scattering Spectra For Different Ocean Components

Table 2.1: Summary of absorption and scattering characteristics of seawater [2]

Compositions	Absorption coefficient	Scattering coefficient
Water	Invariant at constant temperature and pressure. Strongly depends on λ	Rayleigh scattering. Small variance compared with absorption. Strongly depends on λ
Sea salts	Negligible in visible spectrum. Increase towards short λ	Rayleigh scattering Doesnot depend on λ
CDOM	Variable with the density of CDOM. Increase towards short λ	Negligible
Plankton and detritus	Variable with the density of plankton and detritus. Increase towards short λ	Mie scattering. Variable with the density of plankton and detritus. Increase towards short λ

Based on the attenuation coefficient that has been introduced, Beer-Lambert law provides the simplest and most widely used scenario to describe the light attenuation effects in underwater environment [46] as

$$I = I_0 e^{-c(\lambda)z}$$

where I_0 is the power of transmitted light, z denotes the light transmission distance, I represents the power of light after transmitting z distance, and $c(\lambda)$ stands for the attenuation coefficient. The exact value of attenuation coefficient $c(\lambda)$ will change with different water types and water depth. The typical values of $a(\lambda)$, $b(\lambda)$, and $c(\lambda)$ associated with four major water types are given in Table.

In pure seawater, absorption is the main limiting factor, the low scattering coeffi- cient makes the beam free from divergence. In clear ocean waters, there is a higher concentration of

dissolved particles that affects scattering. In coastal ocean water, high concentrations of plankton, detritus and minerals are the dominant sources of absorption and scattering. Turbid harbor water has the highest concentration of dissolved and in-suspension matters, which will severely attenuatethe light propagation 37. More details of water types and variations of attenuation coefficient with other parameters such as depth, pressure, and salinity can be found in 5, 30, 44, 48, 49 .

Table 2.2: Typical values of $a(\lambda)$, $b(\lambda)$, and $c(\lambda)$ for different water types

Water types	$A(\lambda)$ (m^{-1})	$b(\lambda)$ (m^{-1})	$c(\lambda)$ (m^{-1})
Pure sea water	0.053	0.003	0.056
Clear ocean water	0.114	0.037	0.151
Costal ocean water	0.179	0.219	0.298
Turbid harbor water	0.295	1.875	2.17

From (2.4) and (2.7), we know that the Beer lambert's law contains two implicit assumptions. First, the transmitter and receiver are perfectly aligned. Second, all the scattered photons are lost even though in reality some of the scattered photons can still arrive at the receiver after multiple scattering events. This assumption severely underestimates the received optical power, especially in the scattering dominant situation. In order to describe the scattering effects more accurately, another important IOP volume scattering function (VSF) is introduced. It is defined as

$$\beta(\theta, \lambda) = \lim_{\Delta D \to 0\ \Delta\Omega \to 0} P_S(\theta, \lambda)\ \Delta D \Delta\Omega$$

where $P_S(\theta, \lambda)$ is the fraction of incident power scattered out of the beam through an angle θ into a solid angle $\Delta\Omega$ centered on θ (Figure 2.1).

VSF is the scattered intensity per unit incident irradiance per unit volume of water. In the view of physics, the VSF can also be interpreted as the differential scattering cross section per unit volume 36.Integrating $\beta(\theta, \lambda)$ over all directions (solid angles) gives the scattering coefficient.

To this end, we have introduced the concept of absorption and scattering coefficients, Beer Lambert's law, as well as VSF. These concepts provide a theoretical basis for more complex UWC channel models 37. In a UWC link, the optical signal launched from the transmitter will experience various losses before reaching the receiver. They include system loss introduced by transceivers, link loss results from water attenuation, geometric misalignment, and water turbulence. Since the loss introduced by the transceiver is mainly characterized by device parameters and design specifications, it is challenging to characterize the loss in a comprehensive and uniform approach. Thus, in Sections 2.2, 2.3 and 2.4, we will focus on the modeling techniques of the aforementioned losses in UWC links.

2.2 MODELING OF AQUATIC OPTICAL ATTENUATION IN UWC

As we have presented in Section 2.1, without considering the link configuration, transceiver architecture and alignment condition, the two major IOPs that will attenuate light propagation in UWC systems are absorption and scattering. Thus, the modeling of UWC aquatic optical link attenuation can be regarded as a task that accurately describes the absorption and scattering effects with specific link configurations. In the remaining of this section, we will introduce the models of aquatic optical attenuation in two categories: LOS configuration and NLOS configuration

2.2.1 Aquatic Optical Attenuation in Los Configuration

For simplicity, several researchers utilized the Beer Lambert's law to model LOS UWC. In55 and 56, the authors evaluated the performance of a UWC system based on Beer Lambert's law in different water types and different communication ranges. The impacts of environmental variability, such as variations of refractive index with depth, were taken into account.Another general theoretical model of aquatic optical attenuation in UWC is radiative transfer equation (RTE). As we have presented in Section 2.1, the VSF is an important IOP that describes the scattering characterizations of photons.

However, the VSF is difficult to be measured in practice Furthermore, the VSF can only determine the scattering properties of a single photon at one This assumption severely underestimates the received optical power, especially in the scattering dominant situation single refractive index condition. It's not suitable to model the scattering properties of large number of photons 35.

Considering these two facts, most UWC researchers employ RTE in their UWC channel modeling research. Without considering the temporal dispersion of light, the typical two-dimensional RTE can be expressed as

$$\rightarrow n \cdot \nabla L(\lambda, \rightarrow r, \rightarrow n) = -cL(\lambda, \rightarrow r, \rightarrow n) + \int 2\pi \beta(\lambda, \rightarrow n, \rightarrow n^{j}) L(\lambda, \rightarrow r, \rightarrow n) d\rightarrow n^{j} + E(\lambda, \rightarrow r, \rightarrow n) \quad (2.12)$$

where $\rightarrow n$ is the direction vector, ∇ is the divergence operator, $L(\lambda, \rightarrow r, \rightarrow n)$ denotes the optical radiance at position $\rightarrow r$ towards direction $\rightarrow n$, $\beta(\lambda, \rightarrow n, \rightarrow n^{j})$ is the VSF, and $E(\lambda, \rightarrow r, \rightarrow n)$ represents the source radi- ance. RTE is capable of describing the energy conservation of a light wave that is passing through a steady medium 59, 60. The derivations of RTE are complex and lengthy, and they can be found in 61. The RTE can be solved both analytically and numerically. Since the RTE is an integro-differential equation involving several independent variables 58, 60, it is difficult to find an exact analytical solution. Thus only few analytical RTE models have been proposed in recent years. In 62, Jaruwatanadilok devised an analytical solution of RTE employing the modified Stokes vector. This model takes both multiple scattering and light polarization effects into account. Based on this model, numerical results show that the ISI and BER are as functions of data rate and link distance. This finding can be further used to predict several performance parameters of UWC systems such as the maximum communication distance with certain data rate and BER. In 11 and 63, Cochenour *et al*. proposed a beam-spread function for laser-based UWC by solving the RTE analytically. The small angle approximation was performed to simplify the derivation. This ana- lytical model reveals the relationship between received optical power versus link range for various transmitter/receiver pointing accuracies. It was also validated through watertank experiments.

Besides utilizing analytical solutions, numerical methods are preferred to solve the RTE. In fact, for many practical UWC applications, finding an exact analytical solution of RTE is even more challenging. Moreover, since a series of assumptions and approximations have been made to simply the RTE, the analytical solutions will also suffer from numerous limitations 64. In view of this, most of the researchers focused on developing powerful numerical RTE solvers 46, 60. The most popular numerical approach to solve RTE is Monte Carlo simulation. It is a probabilistic method to mimic the loss of underwater light propagation by sending and tracking large number of photons 65, 66.

The Monte Carlo method benefits from its easy programming, accurate solution and high flexibility, but it also suffers from random statistical errors and low simulation efficiency 36. In 67, Leathers *et al*. from the U.S. Naval Research Laboratory (NRL) reported a practical guide to generate Monte Carlo computer simulations for typical ocean optics applications. This method has been referred by many other UWC researchers and has been proved to be robust.

In recent years, lots of researchers have employed Monte Carlo approach to solve the RTE or study the characterization of UWC channels. In 68, Li *et al*. built a Monte Carlo simulator to model the impulse response of UWC channel. Within this simulator, several receiver parameters such as aperture size and field of view (FOV) were taken into account. The authors utilized this Monte Carlo simulator in order to evaluate the channel capacity of a UWC system with different link distances, water conditions, and transceiver parameters 69. Simulation results indicate that the bandwidth of UWC for clean water, coastal water and harbor water are on the order of hundreds of MHz, tens of MHz and MHz respectively 69. Chadi *et al*. from Institut Fresnel utilized a Monte Carlo approach to solve the RTE and provided a channel model that can be used to appropriately predict different design parameters of UWC systems 37. As a continuance of 37, the authors in 50 proposed a channel impulse response of UWC system by solving the RTE through Monte Carlo simulation. The authors quantified the channel time dispersion for different water types, link distances, and transmitter/receiver characteristics. A two-dimensional HG phase function was employed to model the VSF as. . This method has been referred by many other UWC researchers and has been proved to be robust.

$$P_{T\,T\,HG}(\theta) = \alpha P_{HG}(\theta, g_{F\,WD}) + (1-\alpha)\, P_{HG}(\theta, -g_{BKW\,D})$$

where $P_{HG}(\cdot, \cdot)$ is the HG function defined in (2.11); α is the weight of the forward-directed HG function; and $g_{F\,WD}$ and $g_{BKW\,D}$ are the asymmetry factors for the forward- and backward-directed HG phase functions, respectively. Based on this numerical channel model, the authors con- cluded that the channel time dispersion can be neglected when operating at a moderate distance (20m) in a clean water environment. However in highly turbid water, the channel time dispersion can impact the data transmission when operating over a large distance It is a probabilistic method to mimic the loss of underwater light propagation by sending and tracking large number of photons 65, 66.

Carlo simulation and experimental measurements can also be found in 51. The authors devised a numerical Monte Carlo simulation tool that is capable of computing received power of a UWC system by considering the receiver aperture size, FOV, and pointing-tracking losses. This simulator is based on modeling a complex probability density function (PDF) (such as the lightfield distribu- tion underwater) by its known individual components (such as the scattering distance of photons in water) 51. By randomly sampling these known processes, the unknown PDF can be approximated using these discrete samples 51. The accuracy of this simulator was validated through comparing the simulation results with the experimental data from 11, 71. The author in also made the Matlab source code of this simulation tool available to the public.

Besides the probabilistic Monte Carlo approach, there are also two deterministic methods that can be used to solve the RTE numerically: the discrete ordinates method and the invariant imbed- ding method 5, 46. But only few researchers employed these two approaches as alternatives of Monte Carlo simulation. Li *et al*. developed an efficient RTE solver based on the deterministic numerical approach. This solver employs the matrix free Gauss-Seidel iterative method in order to calculate the received power of UWC systems. It can also process highly forward peaked VSF that can not be handled well by the discrete ordinates approach. According to the simulation results, this method can achieve the same accuracy as the Monte Carlo approach but with a much shorter simulation time. The referred Matlab source code of this method can be found in the appendix of 59.

The majorities of aquatic optical attenuation models for UWC are based on solving the RTE. However, instead of solving RTE, several stochastic models have also been proposed from the probabilistic nature of photon trajectory. In 73, Zhang *et al.* from Tsinghua University demonstrated a stochastic channel model to represent the spatial-temporal probability distribution of propagated photons for non-scattering and single scattering ^{4} components of UWC links. The authors adopted the HG function as the probability density function of light scattering angle to simplify the analysis. The proposed stochastic model also exhibited reasonable agreement with the numerical results of Monte Carlo simulation. Based on 73 the same research group further proposed a more general stochastic UWC channel model in 74 67, Leathers *et al*. from the U.S. Naval Research Laboratory (NRL) reported a practical guide to generate Monte Carlo computer simulations for typical ocean optics applications.

This method has been referred by many other UWC researchers and has been proved to be robust.by taking into account of all three components of propa- gated photons, which include non-scattering, single scattering and multiple scattering components.

This comprehensive channel model fits well with the Monte Carlo simulations in turbid water environment, such as in coastal or in harbor waters. Following the similar stochastic approach of 73 and 74, the Tsinghua researchers also presented a closed-form expression for the angle of arrival (AOA) distribution in 75. This AOA model characterizes how the received intensity of ballistic and single scattering components is distributed over AOA with respect to unit transmission power 75. Numerical results have validated the proposed AOA distribution by Monte Carlo approach in clear and turbid coastal and harbor water with relatively short link range.

Semi-analytical modeling approach has also been employed by several UWC researchers. In76 and 77, based on the results of a Monte Carlo simulation, Tang *et al*. adopted a closed form double-Gamma function to represent the channel impulse response of the UWC76 as $h(t) = C_1 \Delta t e^{-C} 2\Delta t + C_3 \Delta t e^{-C} 4\Delta t, \ (t \geq t_0)$ (2.14)

where $\Delta t = t - t_0$. t is the time scale and $t_0 = L/v$ is the propagation time which is the ratio of link range L over light speed v in water 76. The parameter set (C_1, C_2, C_3, C_4) in (2.14) can be computed from Monte Carlo simulation results as 76

$$(C_1, C_2, C_3, C_4) = \arg\min \int [h(t) - h_{mc}(t)]^2 \, dt \qquad (2.15)$$

where $h(t)$ is the double Gamma functions model in (2.14) and $h_{mc}(t)$ is the Monte Carlo simulation results of impulse response; arg min(·) is the operator to return the argument of the minimum. Eq. (2.15) can be solved through a numerical curve fitting approach 76. This semi-analytical impulse response is capable of describing the temporal dispersion of light in turbid underwater environments. It can be used to carry out a performance evaluation for calculating the BER and 3-dB channel bandwidth of a UWC system. As an extension of 76 and 77, the authors applied a similar curve fitting approach to derive the the impulse response for LOS UWC links with multiple-input multiple-output (MIMO) configuration 78 Weighted double Gamma functions have been derived as the impulse response of a 2-by-2 LOS MIMO UWC system in turbid water environment.

During the past ten years, a lot of research has focused on UWC aquatic optical attenuation modeling. However, to this date, only a few models are capable of providing an end-to-end simulator for the UWC designers 64. There's still several "barriers" between the UWC channel modelers and hardware engineers 64. In 79 Doniec *et al*. presented an end-to-end model that can simulate the signal strength and communication distance in any propagation directions. This generic model incorporates all the components of a UWC system that includes information of light source, detectors, amplifiers, and analog-to-digital converters 79. The authors also verified this model through an autonomous underwater optical robotic system. Since this model takes into account all the relevant components of a UWC system as well as the attenuation properties of water, it provides a direct and complete reference for UWC designers to estimate the overall system performance.

2.2.2 Aquatic Optical Attenuation in Nlos Configuration

As shown in Figure 1.3(d), in NLOS implementations, transceivers can utilize reflection of the sea surface to overcome link obstacles. Compared with channel modeling of LOS UWC, investigations of NLOS UWC channel modeling have received less attention. Light propagation in NLOS configuration experiences the same attenuation effects as in LOS configuration. The major difference between LOS and NLOS channels is the reflection effects introduced by wavy sea surface. Thus accurately describing the reflection effect of sea surface is considered as the most critical part of NLOS channel modeling. Several models that describe the slopes of random sea surface can be found in 10, 80, 81. Similar to channel modeling work of LOS configuration, channel models of NLOS link can also be derived both analytically and numerically. To the best of our knowledge, most channel models of NLOS configuration were derived through numerical approaches such as through Monte Carlo simulations.

As an example of an analytical approach, Shlomi *et al*. in 23 and 24 proposed a novel concept of NLOS UWC network. Each node inside this network can communicate with each other through reflection at the ocean-air interface. Communication from one single node to multiple nodes can also be achieved. The authors derived a mathematical model for the NLOS channel by considering the link attenuation, sea surface slopes and receiver FOV. Numerical simulation was also performed to test the validity of this NLOS UWC channel model.

Simulation results show that an increase in node separation distance dramatically increases the BER of the NLOS UWC system. By applying the numerical Monte Carlo method, the authors of 25 proposed a path loss model for NLOS UWC links. The effects of both random sea surface slopes and scattering properties of seawater have been taken into account. Numerical results suggest that the random surface slopes induced by wind or other turbulent sources may strongly corrupt the received signal. However, this effect can be alleviated when the received signal contains multiple dominant scattering light components. In 82 and 83, Jagadeesh *et al*. proposed an impulse response for NLOS UWC based on Monte Carlo simulation. A two-dimensional HG angle scattering function was employed in this simulation process in order to model the multiple scattering effects of light. Based on this impulse response, the authors also evaluated the system performance with different water types and receiver FOV.

2.3 MODELING GEOMETRIC MISALIGNMENT OF UWC

As introduced in Section 1.2, the undiffused point-to-point UWC links suffer from temporal misalignment. This undesired effect will degrade the system performance and induce temporal communication interruptions. In fact, link misalignment is unavoidable in any UWC systems, and there are three major reasons that will tighten the system alignment requirements.

Limitations of transceivers: In order to achieve a higher data rate and longer communication range, many UWC applications utilize the laser diode and photo diodes as transmitters and receivers respectively. However, due to the narrow divergence angle of laser diodes and limited FOV of photo diodes, these UWC systems require precise alignment.

Relative motions caused by underwater vehicles, ocean current, and other turbulent sources: UWC links suffer from severe misalignment when communicating with an AUV or ROV. Since the AUV or ROV keeps moving, the transceivers should always keep tracking with each other. Thus, link misalignment is more likely to occur. Ocean currents and wind can introduce random movements of transceivers in underwater environment, possibly causing link interruptions.

Variations of refractive index: The refractive index will change with water depth, temperature, salinity, and other environmental conditions. This phenomenon usually occurs in surface-to-bottom UWC links and will cause the non-straight light propagation, thus aggravate link misalignment of UWC 30.

Similar to the modeling work of UWC aquatic optical attenuation, both analytical and numerical methods can be implemented in the modeling of UWC link misalignment. For the analytical cases, without focusing on the pointing error caused by slight jitter of the transceivers, the authors in 84 employed the beam spread function to model the link misalignment when the receiver deviates in a larger region 11, 84

$$BSF(L,r) = E(L,r)\exp(-cL) + \int_0^\infty E(L,v)\exp(-cL) \times \left\{\exp\left[\int_0^L bs\left(v(L-z)\right)dz\right] - 1\right\} J_0(vr)vdv \tag{2.16}$$

where *BSF* (*L, r*) is the irradiance distribution of the receiver plane; *E*(*L, r*) and *E*(*L, v*) are the irradiance distributions of the laser source in spatial coordinate system and spatial frequency do- main, respectively 11; *L* presents the distance between the source and the receiver plane; *r* is the distance between the receiver aperture center and the beam center on the receiver plane which is assumed to be perpendicular to the beam axis; *b* and *c* are the attenuation and scattering coeffi- cients respectively; *s*(*v*) is the scattering phase function. Through this model, the authors evaluated the BER performance of UWC under misalignment condition. Numerical results indicated that, regardless of water type, an appropriate amount of misalignment will not cause severe performance degradation with sufficiently large transmission power. A similar conclusion was also drawn from the experiment of 85. As an extension of 84, Dong *et al*. in 10 have presented a model of random sea surface slopes that concerns the link pointing errors caused by slight jitter of the transceivers for a vertical buoy-based UWC system. The PDF of random sea surface slopes is expressed as [10] Similar to the modeling work of UWC aquatic optical attenuation, both analytical and numer- ical methods can be implemented in the modeling of UWC link misalignment. For the analytical results.

$$P(s_x, s_y) = \frac{1}{2\pi\sigma_u\sigma_c}\exp\left[-\left(\frac{s_x^2}{2\sigma_u^2} + \frac{s_y^2}{2\sigma_c^2}\right)\right] \tag{2.17}$$

where $s_x = \partial z/\partial x$ and $s_y = \partial z/\partial y$ are defined as wave slopes of up/downwind and crosswind directions in the Cartesian coordinate (*x, y, z*) respectively; σ^2 and σ^2 denote the mean square slope in the up/downwind and crosswind directions, respectively.

The authors employ this model and beam-spread function to evaluate the BER performance of the system. Numerical results suggest that the BER deteriorates as the pointing errors increase. This performance degradation can be released through an increment in the seawater turbidity. Zhang *et al*. have also employed a similar PDF of random sea-surface slope as 10 but in the form of angle to model the pointing errors of buoy- based downlink UWC systems 86. The authors utilized this model and evaluated the channel capacity of downlink buoy-based UWC multiple-input multiple-output systems. Numerical results suggest that more turbid water, larger link range and larger inter-spacing may reduce the channel capacity, and meanwhile more turbid water and larger link range can weaken the effects of random slopes on the channel capacity 86.

2.4 MODELING LINK TURBULENCE OF UWC

Numerical methods have also been employed to model UWC link misalignment. By using a Monte Carlo approach, the authors of 87 studied the impact of link misalignment on the received power of a point-to-point LOS UWC system. This numerical model was validated through water- tank experiments. Since misalignment effects in LOS UWC can also be caused by variations of refractive index. In 30 and 49, Laura *et al*. proposed a profile of the refractive index with the variation of depth. This profile was then used in a numerical ray-tracing simulation in order toevaluate the tolerence of UWC link offset. From the numerical results, a 0.23m link offset was allowed for 500nm laser with 0.57 degree FOV and 200m link distance. This work provides an effective reference for modeling link misalignment induced by refractive index variations 88.Turbulence in UWC is defined as the event that makes water experience rapid changes in the refractive index 22.

This phenomena is commonly caused by ocean currents which will in- duce sudden variations in the water temperature and pressure. Most studies on UWC channel modeling have focused on providing an accurate description of absorption and scattering effects, but the impact of underwater optical turbulence is commonly ignored. In fact, underwater optical turbulence can also cause considerable degradation to the performance of a UWC system. Thus, more attention should be paid to this subject. The modeling of underwater optical turbulence is mainly based on research results of atmospheric optical turbulence channel models in free-space optical communications. Considering the similarity of underwater optical turbulence and atmospheric optical turbulence, several researchers directly applied or modified .

CHAPTER 3

UWC CHANNEL MODULATION AND CODING TECHNIQUES

In this chapter, we will first give a brief introduction of several digital modulation techniques that implemented in UWC systems. The advantages and limitations of each modulation scheme will be presented. Then, we will discuss the channel coding techniques of UWC. Finally, we will summarize this chapter and classify the related literatures on UWC channel modulation and coding topics.

3.1 MODULATION SCHEMES OF UWC

UWC channel modulation techniques have attracted much attention in recent years due to its capability to impact the system performance considerably. Since UWC can be regarded as implementing FSO in underwater environment, the conventional intensity modulation (IM) techniques that used in FSO communication systems can also be applied to UWC systems. On-off keying (OOK) modulation is the most popular and simplest IM scheme in FSO communication system. This modulation scheme can also be implemented in UWC systems.

The OOK modulation is a binary level modulation scheme. During an OOK transmission, an optical pulse which occupies part of or entire bit duration represents a single data bit “1”. On the other hand, the absence of an optical pulse represents a single data bit “0”. There are two pulse formats in OOK modulation scheme: return-to-zero (RZ) format and non-return-to-zero (NRZ) format. In the RZ format, a pulse with duration that only occupies a part of the bit duration is defined to present “1”; however, the pulse duration occupies the whole bit duration in the NRZ scheme. The RZ-OOK has been proved having higher energy efficiency than the NRZ-OOK, but at the expense of consuming more channel bandwidth.

In practical optical communication systems, the choice between RZ and NRZ formats in OOK modulation depends on the specific performance requirements and system constraints. The NRZ-OOK format is simpler to implement and requires less bandwidth, making it suitable for bandwidth-limited systems. However, its longer pulse duration can lead to intersymbol interference (ISI) at high data rates due to pulse overlapping. On the other hand, RZ-OOK, with its shorter pulse duration, offers better timing precision reduced

Which enhances signal clarity and system performance, especially in high-speed transmissions. This makes RZ-OOK a preferred choice in scenarios where signal integrity and energy efficiency are critical, despite its higher demand for bandwidth. Additionally, advanced RZ pulse shaping techniques can further optimize performance by minimizing dispersion effects in long-distance optical fiber communication.

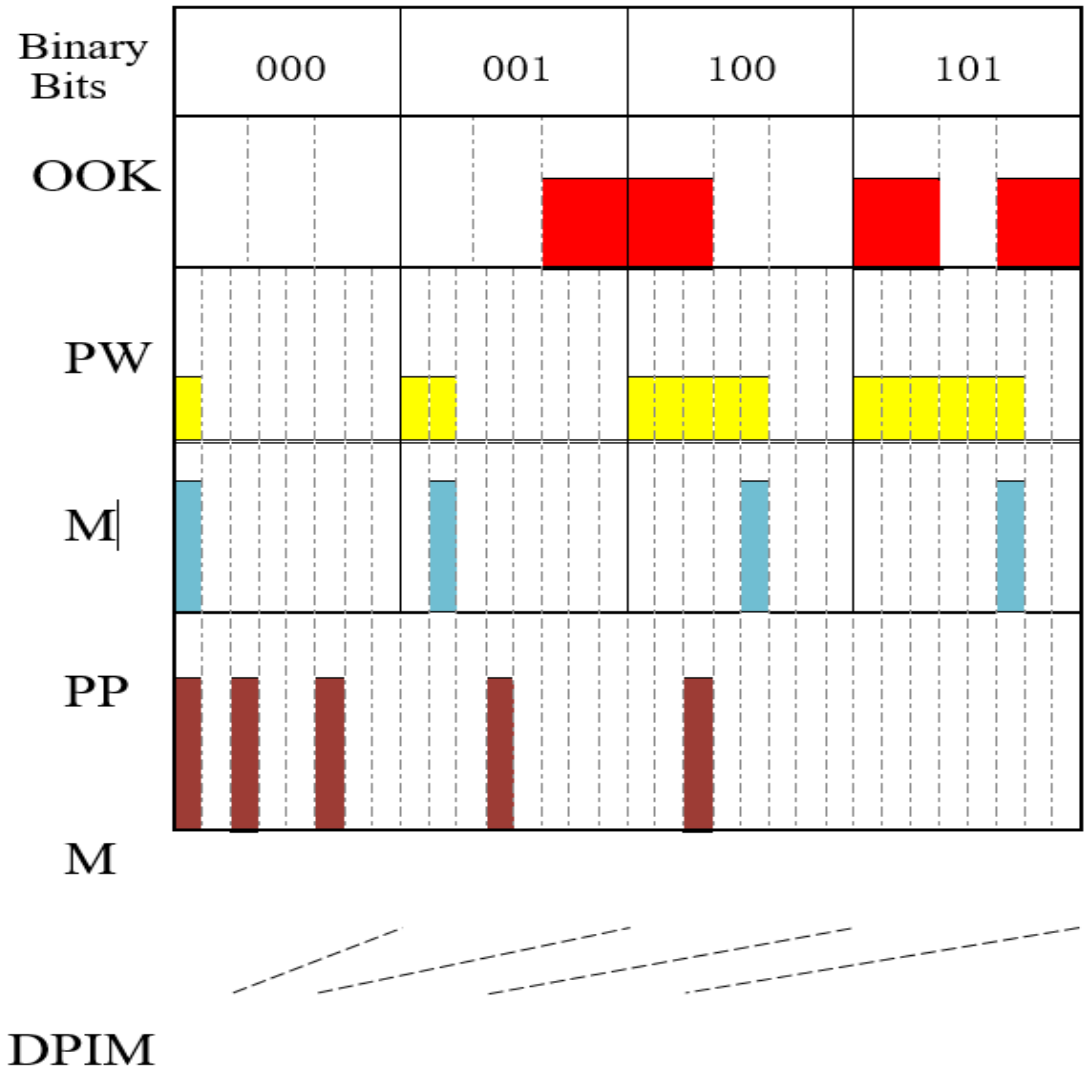

Figure 3.1: Illustration of OOK, PWM, PPM and DPIM.

The DT is determined based on the estimation of channel fading. Several channel estimation techniques of FSO communication systems such as pilot symbol method, symbol-by-symbol maximum likelihood (ML) method, and ML sequence method 98 can also be employed by the UWC OOK systems. The two major drawbacks of UWC OOK scheme are low energy efficiency and spectral efficiency. But considering its simplicity, OOK modulation is still the most popular IM scheme in UWC. It has been implemented in a number of theoretical and experimental UWC research works 62, 99, 100.

Pulse position modulation (PPM) scheme is another popular modulation technique used in UWC systems. Compared with OOK modulation, PPM has much higher energy efficiency and doesn't require dynamic thresholding, but at the expense of lower bandwidth utilization rate and more complex transceivers. In PPM, every transmitted M bits will be modulated as one single pulse in one of 2^M time slots, and the pulse position represents the transmitted information (Figure 3.1). The main drawback of PPM modulation is the tight timing synchronization requirement. Any timing jitters or asynchronization will severely degrade the BER of system. In recent years, several researchers have studied the performance of PPM scheme over UWC channel models. The authors of 101 have investigated the performance of 4-PPM scheme over numerical RTE channel model. They have found that the corresponding BER for PPM scheme is almost equal to that of OOK modulation and with much higher energy and spectrum efficiency. More complex PPM such as 8-PPM or 16-PPM can be used to improve higher bandwidth efficiency. In 102, Sui *et al*. proposed a modified PPM scheme for UWC. This modified PPM can maintain the similar power efficiency and anti-noise performance as the conventional PPM. It also has improved the bandwidth utilization rate of the system. Besides theoretical studies, PPM was also applied in several experimental UWC implementations. The related literatures can be found in 103–109.

Similar to PPM, pulse width modulation (PWM) also utilizes the relative positions of pulses to represent data symbols. In L-ary PWM, optical pulses will only appear in the first L consecutive time slots to represent one symbol.

Off slots depends on the decimal value of the transmitted symbol, and an additional guard slot is commonly added in order to avoid sending consecutive “On” pulses (Figure 3.1) 9. Compared with PPM and PWM which require slot and symbol level synchronization, digital pulse interval modulation is an asynchronous modulation scheme with variable symbol length 98. Furthermore, with variable symbol length, DPIM also has higher spectral efficiency than PPM and PWM 98. The most critical problem of DPIM is the error spread in demodulation. From Figure 3.1, we notice that if an “Off” slot is demodulated as “On”, then all the succeeding symbols will also be wrong. Applications of DPIM can be found in several UWC applications of ROVs and AUVs such as 110–112.

Similar to the comparison of IM schemes that we have made, the authors of 9 also performed a comparison study on different IM techniques for UWC. This comparison included OOK, PPM, PWM, DPIM and other derivative IM schemes such as multi-pulse PPM (MPPM) and differential PPM (DPPM). Simulation results show that with the same link distances, PPM is the most energy efficient modulation scheme. DPIM has better bandwidth efficiency over PPM and OOK but at the expense of more complex demodulation devices. Other similar comparison of IM for UWC can also be found in 108 and 113.

Coherent modulation schemes have also been implemented in several UWC systems. In con- trast to the direct IM schemes, coherent modulations encode the information on the amplitude, polarization or phase of optical carriers. At the receiver side, the same synchronized optical carrier will mix with the received optical signals and accomplish demodulation. Compared with IM, coher- ent modulations benefit from higher receiver sensitivity, higher system spectral efficiency and better rejection on background noise, but at the expense of higher implementation complexity and higher cost 98. Due to the high dispersion effect of seawater, coherent modulation at optical frequencies is difficult to be achieved in UWC systems. In order to overcome this limitation, intensity modu- lation has to be imposed on the pre-modulated signals 114. Typical coherent modulations used in UWC systems include quadrature amplitude modulation (QAM), phase shift keying (PSK), and polarization shift keying (PolSK).

IM schemes such as OOK and PPM. Simulation results have demonstrated that PSK modulation performs the best over other modulation schemes in terms of data rate and BER. But it also suffers from poor power efficiency. A binary PolSK (BPolSK) modulation for UWC has been introduced in 116. In BPolSK, the signal is modulated by changing the polarization of the light. Since po- larization states of light are less sensitive than the amplitude, phase or intensity of optical signals, BPolSK has higher tolerance to underwater turbulence and other channel interference such as am- bient light. This property is ideal for UWC in low SNR environment. PolSK can also be used to suppress backscatter of the transmitter in a duplex system and has better immunity to phase noise of lasers 98, 116. Although PolSK is ideal for optical wireless communications, it still suffers from short transmission distance and low data rate. To overcome these limitations, Dong *et al*. presented a novel polarized pulse position modulation (P-PPM) 117, 118. This modulation scheme combines conventional PPM and PolSK together by transmitting a series of PPM symbol in different polar- ization directions 118. Numerical results show that P-PPM benefits from the virtues of both PPM and PolSK. It can increase the transmission bandwidth and distance of a UWC system.

Another coherent modulation scheme implemented in UWC is the subcarrier intensity modu- lation (SIM). The interest of SIM is the much higher spectral efficiency 9. But SIM also requires complex modulation/demodulation devices and suffers from poor average power efficiency 119. By using SIM, orthogonal frequency-division multiplexing (OFDM) can also be achieved in UWC systems 119, 120. techniques can be applied.

3.2 CHANNEL CODEING OF UWC

As was discussed in the previous chapters, due to the severe absorption and scattering effects induced by sea water, the transmitted optical signal will experience considerable attenuation. This undesirable effect will directly degrade the BER performance of UWC system. In order to mitigate the impact of aquatic optical attenuation and maintain a low BER in low SNR underwater environment, forward error correction (FEC) channel code lower transmitter power requirements or extended link range.

Generally, FEC codes can be divided into two categories: block codes and convolutional codes 121. Researchers have employed several classical block codes into the UWC systems due to their simplicity and robustness. The first block code that implemented in UWC system is the Reed-Solomon (RS) code 122. In 122, Cox *et al*. demonstrated an experimental UWC system that utilized (255, 129) RS FEC code.

This system employed 405 nm laser diode and RZ OOK modulation to achieve a 500 kbps UWC link in a 3.66 meters long water tank. The experimental results suggested that the coded system can reduce the required power to achieve a BER of 10^{-4} by approximately 8 dB compared with an uncoded OOK system. Based on 122, the same research group from North Carolina State University upgraded their system in 123. In the upgraded system, a 5 Mbps UWC link was established also using RS code in three and seven meters long water tanks. The experimental results show that the (255,129) RS and (255,223) RS codes are capable of improving the SNR of received signals about six and four dB respectively at a given BER of 10^{-6}. Another similar experimental UWC system that utilized (2720,2550) RS and SIM can be found in 120. In this system, the (2720, 2550) RS code performed an error correction that reduced the input BER of $1.5 \cdot 10^{-3}$ to 10^{-9}.

Besides the RS code, other classical block code and error-detecting code such as Bose-Chaudhuri- Hocquenghem (BCH) code and cyclic redundancy check (CRC) code have also been implemented in UWC systems to improve the BER performance in low SNR underwater environment. In 124, the authors simulated the anti-noise performance of BCH and RS codes with simple OOK modulation. Numerical results indicated that the RS code outperformed the BCH code in error correction capability, but at the expense of lowering transmission data rate. In 106, a UWC system based on hardware description language (HDL) was demonstrated. In this system, the authors referred the architecture of IEEE 802.15.4 and IEEE 802.11 protocols and implemented CRC code in the medium access control (MAC) layer of the system.

The BER performance at the receiver was improved compared with uncoded systems. Instead of applying one layer of FEC code for byte-level error correction, packet-level error correction coding schemes were also developed to maintain the UWC system. In 79 and 125, Doniec *et al*.

Embedded a two-layer error correction coding scheme into a UWC video transmission system. In this two-layer channel coding scheme, the transmitted video frames were firstly encoded on Manchester codes and Luby Transform (LT) codes to mitigate packet-level losses, then CRC and RS codes will be employed sequentially for byte-level error correction at the physical. Although several block codes are simple to be implemented, they are not capable of providing the optimal performance for UWC, especially in the environment with strong interference. Thus, more complex and powerful channel coding schemes such as low-density parity-check (LDPC) code and Turbo code are employed.

LDPC code is a highly efficient linear block code. It is constructed by employing sparse parity check matrices and can provide an error-correction performance close to the Shannon limit 98. Turbo code is a parallel concatenated code. It combines two or more convolutional codes and an interleaver to produce a block code that can also achieve a BER close to the Shannon limit.

Although lots of research works on implementing LDPC and Turbo codes in FSO communication system have been proposed, there is still little investigation on applying LDPC and Turbo codes in UWC. Everett demonstrated the performance of RS, LDPC and Turbo codes in UWC systems both theoretically and experimentally 126. The author explained the mechanism of RS, LDPC and Turbo codes in details, and compared their performance for UWC such as BER, power efficiency, and link distance extension. This work provides a relatively complete description of implementing channel coding techniq

CHAPTER 4

EXPERIMENTAL SETUPS AND PROTOTYPE OF UWC

In this chapter, we will study the experimental setups and prototypes of UWC from different aspects. Firstly, we are going to introduce several typical LOS/NLOS experimental setups and prototypes of UWC. Secondly, we will review the research of UWC implementations in several specific topics, which include retroreflector, smart transceiver design, UWC for underwater vehicles and the hybrid UWC systems. Finally, we will summarize this chapter and propose the literature classification of experimental UWC systems.

4.1 TYPICAL LOS/NLOS UWC SYSTEMS

As we have mentioned in Chapter 1, although a few commercial UWC products were proposed in the early 2000s, the large scale commercial applications of UWC systems have not been realized so far. Most of the UWC systems are experimental demonstrations and prototypes in laboratory environment. In the remaining of this section, we will provide a comprehensive summary of the recent progress on experimental UWC research. The purpose of this summary is not to introduce all the UWC experimental literatures in details, but to provide a general description of the most recent works on UWC experiments that concern different applications and approaches.

According to the link configurations, experimental setups and prototypes of UWC can be divided into two categories: LOS experimental setups and NLOS experimental setups. Due to the simplicity of implementation, most UWC experimental systems utilize LOS configuration. In Figure 4.1, a typical laboratory LOS UWC system based on intensity-modulation direct-detection is demonstrated. The configuration of LOS UWC link is similar to the FSO communication setups 98. On the transmitter side, the information bits are generated by a personal computer (PC), and then modulated onto optical carriers. In several UWC experiments, the modulated optical signal will be further amplified by an optical amplifier and then transmitted through lens that are precisely. Although lots of research works on implementing LDPC and Turbo codes in FSO aligned to focus the light.

Water tank or pipe is used to model the underwater transmission link. In order to mimic the different refractive condition and turbidity of underwater environment, Maalox is added in the water to act as a scattering agent for attenuating the light beam 94, 127.

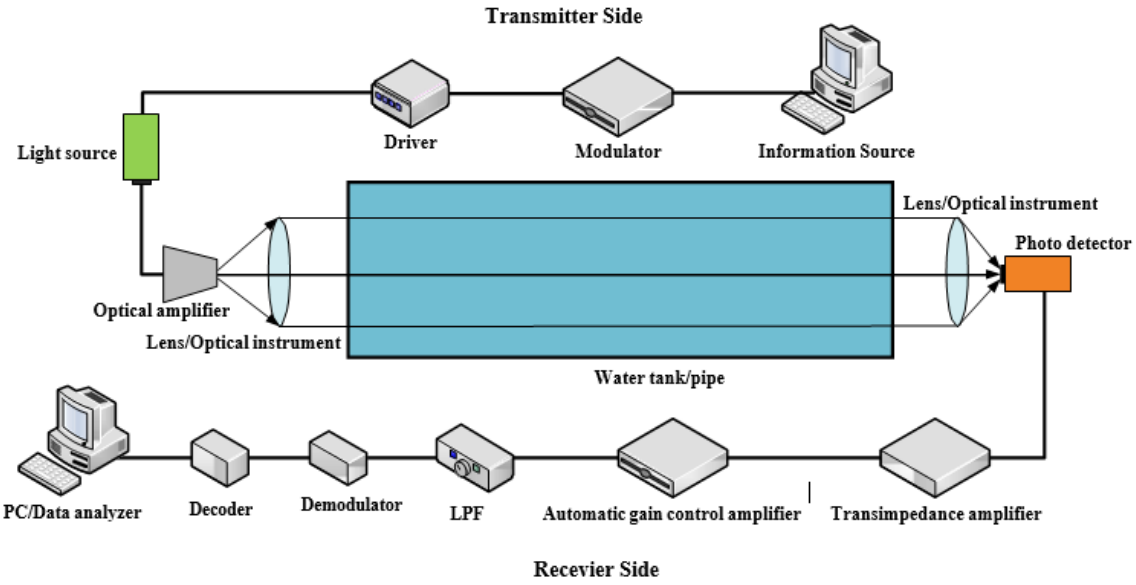

Figure 4.1: A typical laboratory LOS UWC system based on intensity-modulation direct-detection (IM/DD) technique.

On the receiver side, the optical signal will go through an optical filter and focusing lens. It will then be captured by the photodiode. Since photodiode can only transform the variations of light intensity into corresponding current changes, a trans-impedance amplifier is cascaded as the following stage to convert current into voltage. The transformed voltage signals will then go through a low pass filter to reduce the thermal and ambient noise levels 98. Further signal processing programs that include demodulation and decoding will be performed at the last two stages of the receiver. The recovered original data will finally be collected and analyzed by a PC or BER tester for evaluating several important performance parameters such as BER.

There are two light sources that are commonly used in typical UWC experimental systems: (LEDs) and (LDs). As it was stated in Chapter 1, blue or green wavelength has been chosen for the light sources to minimize the aquatic optical attenuation.

Compared with LED, LD has higher output power intensity, better collimated properties, narrower spectral spreading, and much faster switching speeds. But at the expense of higher cost, shorter lifetime and dependence on temperature. Thus LDs are more appropriate to be implemented in applications of high-speed UWC that has strict alignment requirement. In several LD-based UWC applications, optical diffusers are implemented to reduce the system pointing requirements. Compared with the LD-based UWC system without diffusers, this diffused LD-based UWC system can benefit from both high speed and relatively low pointing requirements. On the other hand, since LEDs offer lower output power intensity, wider divergence angles, and lower bandwidths. They can be installed in several diffused UWC applications with short-range, low-speed link requirement.

At the receiver, there are also two types of photodiodes that are widely used in UWC ex- periments: P-i-N (PIN) diode and avalanche photodiode (APD). The major difference between these two devices is in the noise performance. For PIN photodiodes, the dominant noise is thermal noise, while for the APDs, the performance is mainly limited by shot noise 98. Since APD can provide higher current gain, it can be implemented in longer UWC links (tens of meters), but at the expense of more complex auxiliary circuits. Besides PIN diodes and APDs, photomultiplier tubes (PMT) have also been implemented in several UWC experiments 70, 105, 106, 128–131. Compared with photodiodes, PMT benefits from higher sensitivity, higher optical gain and lower noise levels. But it also suffers from high voltage supplies (on the order of hundred volts) and high unit cost. Moreover, PMT is susceptible to shocks and vibration. It can be easily damaged by the overexposure to light. The cost of PMTs are also much higher than photodiodes. Thus PMTs are commonly used in static experimental UWC systems. Based on the typical LOS UWC link configuration and the critical devices that we have introduced, lots of experimental UWC links fo- cusing on channel model verification and system performance analysis have been proposed in recent years. Since LED benefits from its low cost and stable performance in various environments, several researchers preferred to employ it as the light sources in experimental UWC systems 109, 120, 124, 132. In 7, Chancey proposed a UWC system based on high power Gallium Nitride LEDs. This experimental demo is capable of achieving 10 Mbps video transmission over a distance of 12 meters.

Also in 8, Simpson from the North Carolina State University demonstrated a UWC system with signal processing capabilities that utilized high-power LED as the light source. Experimental results show that 1 Mbps data rate is achievable over a distance of 3.66 meter long. Similarly, the author of 133 has also developed a UWC system that utilized a high-power blue LED as transmitter and a blue enhanced photodiode as receiver. This system successfully accomplished a 3 Mbps data

4.2 RETROREFLECTORS OF UWC

Retroreflector is an optical device that can reflect arbitrary incident light back to its source (Figure 4.2). Utilizing this beneficial characterization, a modulating retroreflector UWC system was introduced. In the modulating retroreflector link (Figure 4.3), the active transceiver projects a light beam into the retroreflector. During the reflection process, the modulator will modulate the light beam and add information on it. This information will later be captured and demodulated by the active transceiver. The most significant advantage of modulating retroreflector UWC system is that most of the power consumption, device weight, volume and pointing requirements are shifted to the active end of the link, thus the passive end will benefit from small dimensions, relatively low power and pointing requirements 146. There are lots of sensor nodes and underwater vehicles in UWSNs. Each sensor node and underwater vehicle is required to have long enough cruising time due

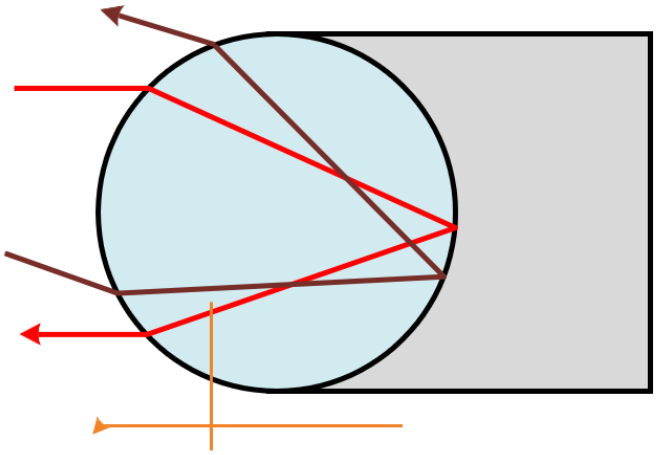

Figure 4.2: Demonstration of corner and spherical retroreflectors.

In this sense, modulating retroreflector becomes an attractive choice. In addition to the challenges that involved in a direct UWC link such as absorption and scattering, retroreflector-based UWC systems have several additional limitations. Unlike the typical UWC links, the retroreflector based UWC links have to transmit through the underwater channel twice.

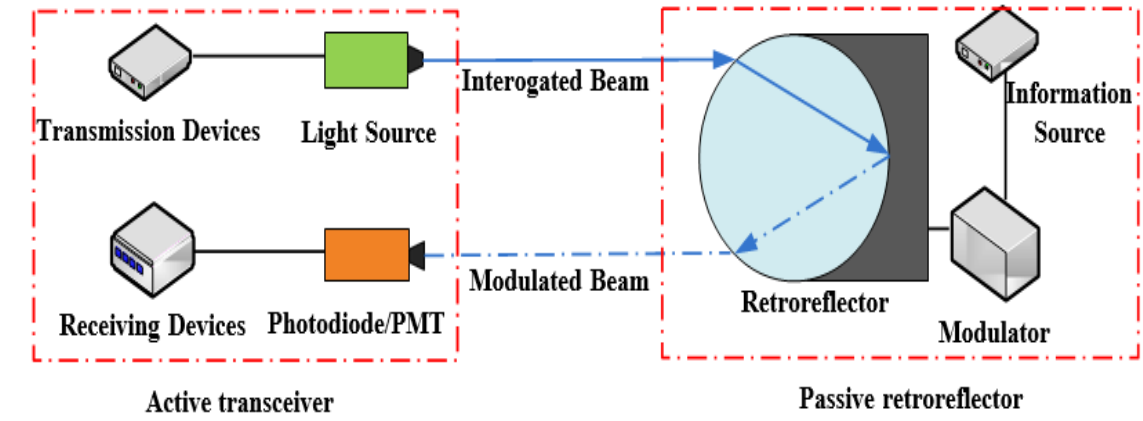

Figure 4.3: Modulating retroreflector link.

So the link will experience higher attenuation and interference. Furthermore, the backscattered light generated from the interrogating beam can be significant in turbid water where it will eventually surpass the desired retro-reflected signals to the difficulty of recharging battery. In this sense, modulating retroreflector becomes an attractive choice. In addition to the challenges that involved in a direct UWC link such as absorption and scattering, retroreflector-based UWC systems have several additional limitations. Unlike the typical UWC links, the retroreflector based UWC links have to transmit through the underwater channel twice, so the link will experience higher attenuation and interference. Furthermore, the backscattered light generated from the interrogating beam can be significant in turbid water where it will eventually surpass the desired retro-reflected signals. In the modulating retroreflector link (Figure 4.3), the active transceiver projects a light beam into the retroreflector. During the reflection process, the modulator will modulate the light beam and add information on it.

4.3 SMART TRANSCEIVERS

As shown Figure 4.1, in a UWC system, the information waveforms are generated by a source and then transferred by an optical transmitter through the water channel to a specific destination. At the other end of the link, the receiver will collect the optical signal and recover the original information. Although the transmission wavelength is carefully selected in blue/green transparent window to minimize the attenuation effect of sea water, several other factors such as misalignment will still severely degrade the link performance. As we have stated in Chapters 1 and 2 , most UWC systems utilize point-to-point configuration, and thus precise pointing and tracking requirements are necessary. However, link misalignment is an inevitable phenomena in underwater environment, any variations of refractive index or turbulence of ocean can cause link misalignment and interrupt communication.

Especially in mobile UWC applications such as AUVs and ROVs, the two ends of a link are all in nonstatic condition, which makes the alignment more difficult to be achieved. Conventionally, there are three common methods to relief the pointing requirements of a UWC system: using diffused light beam, increasing receiver aperture size, or implementing a dedicated gimbal system. Diffused light beam can effectively increase the illuminated area of a light source, but the communication range also shrinks. Although large aperture can increase the receiver FOV and it has already been implemented in several UWC systems such as 142, the extra introduced ambient light and limited transceiver size requirement will still restrict the application of this method. Dedicated gimbal system can be used in several applications that have less size limitation and energy requirements, but for compact UWC systems that don't have much volume.

Considering the limitations of each compensation method that we have introduced, a compact adaptive smart UWC transceiver that can relax the misalignment requirement with minimized volume and energy cost. In 152, Simpson *et al*. proposed a novel UWC front-end that intro- duced the concept of smart transmitter and receiver. The smart quasi-omnidirectional transmitter can estimate the water condition according to the backscattered light captured by the adjacent smart receiver. Based on specific water conditions.

The transmitter can also electronically switch the beam direction according to the angle of arrival of detected signal. On the receiver side, segmented lens array architecture was implemented to increase the total FOV. By using the information of angle of arrival estimation, the smart receiver can also adjust and steer the FOV towards the direction of desired signals to improve the the SNR of the received signal. Moreover, the CDMA technique has also been implemented in both transmitter and receiver ends to reinforce the system performance in multi-user environment. The authors installed the prototyping smart transceivers in a 3.66-meter long laboratory water tank to evaluate the system performance.

Experimental results demonstrate that the smart system can effectively increase the total FOV of the receiver. The preliminary algorithm for angle of arrival estimation and backscatter estimation was also verified to work properly. Other performance aspects such as diversity combining and multi-user CDMA approach were also tested and proved to be effective. This novel trial of smart transceivers provides an adaptive solution to handle the impact of dynamic nature of underwater environment to the UWC systems. It can be applied to different underwater platforms such as AUVs, ROVs, and other sensor nodes embedded with UWC system. Several theoretical research works focusing on smart or adaptive UWC transceivers were also proposed. In 107, Tang *et al*. presented an adaptive gain control scheme for UWC receivers based on APD. The authors derived a close-form expression that can describe the relationships of optimal gain of APD, link range and receiver offset distance. This result can be further applied to practical design of UWC transceiver for improving the link reliability. Unlike the typical UWC links, the retroreflector based UWC links have to transmit through the underwater channel twice

4.4 UWC FOR UNDERWATER VEHICLES

With the increasing demands of human underwater activities, underwater vehicles such as AUVs and ROVs have been widely applied to perform different tasks such as undersea resource exploration, wreck rescue missions and maintenance of oil production facilities. In the perspective of commu- nication methods, underwater vehicles can be divided into three categories: tethered underwater vehicles, wireless underwater vehicles, and hybrid underwater vehicles. Tethered underwater vehi-cles are usually controlled robots that connected to the surface control platform through an optical fibre or electrical cable.

The tethered system has long endurance time and can provide reliable high-speed data communication, but at the expense of higher manufacture cost and limited opera- tion range. On the other hand, conventional wireless underwater vehicles are usually autonomous operated robots that utilize acoustic wave as the viable communication carrier 153. Since this kind of vehicle is free from the limitations of connection cable, it has more flexibility and can operate in a vast area. The bottle neck of this approach are the low bandwidth, high latency, and complex energy-consuming acoustic transceivers. Hybrid underwater vehicles integrated both tethered and wireless systems together 154, 155.

It has the optimal flexibility and reliability, but it's not suitable for the large-scale implementations in UWSNs due to the high unit cost, bulky instrumentations, and large number of cables. In order to satisfy the needs of UWSNs for compact, endurable, and high-bandwidth under- water vehicles, several researchers have embedded UWC into AUVs and ROVs to overcome the limitations of conventional underwater vehicles. A team from the Computer Science and Artifi- cial Intelligence Laboratory (CSAIL) of MIT firstly proposed a prototyping AUV system called autonomous modular optical underwater robot (AMOUR) 156. The AMOUR was designed to perform tasks that including underwater monitoring, exploration, and surveillance. Since AMOUR is based on a stack-up modular design approach, it also has the capabilities to deploy and recover sensor nodes in the sensor networks.

The earliest version of AMOUR employs LEDs as the light source and can achieve one Kbps data rate over a distance of two meters. After the presentation of the first AMOUR prototype, CSAIL researchers upgraded the AMOUR system. Several new fea- tures based on UWC such as remote control, localization, and time division multiplexing access (TDMA) have been implemented into this underwater vehicles systems 157, 158. In [159], the researchers demonstrated a cooperative UWSN that employed AMOUR, another different kind of AUV named Starbug and several underwater sensor nodes 160. During the experiment, cooper- ative tasks such as data transmission, cooperative localization and navigation, as well as physical connection were performed. This work has proved the feasibility of cooperations among different underwater vehicles and sensor nodes. It also verified the plausible approach to achieve long-term operation of UWSNs.

In 112, an upgraded underwater vehicle system AMOUR VI that embed- ded with UWC module to achieve real-time control link was demonstrated. In this experiment, the CSAIL researchers used blue/green LEDs as light source and tested the system in a shallow swimming pool where ambient light existed. Human input device was used to control the orienta- tion of the vehicle. Compared with the conventional acoustic ROVs which has a data rate up to hundred Kbps and latencies of hundred milliseconds, this UWC system can achieve data rate on the order of Mbps and latencies on the order of one millisecond in a range of tens of meters. The architecture of the vehicle is compact. Both the transmitter and receiver modules are sealed in a transparent plastic cylinder with approximate length of 30cm and weight of two kilograms. The vehicles can also move in arbitrary directions with the embedded thruster system. The details of this thruster algorithm and its corresponding configurations were presented in 161. Besides these research results that were proposed by MIT CSAIL, other UWC research groups also presented several demos and prototypes on optical wireless underwater vehicles such as 6, 162, 163. Hybrid communication systems which included both acoustic and optical modules were also implemented in several underwater vehicles 164, 165. We will introduce them in the following section.

CHAPTER 5
SOFTWARE REQUIRED

5.1 SOFTWARE

To support the development of underwater wireless communication technology, MATLAB serves as an invaluable tool due to its robust capabilities in simulation, analysis, and algorithm development. MATLAB's powerful environment allows researchers and engineers to design and optimize communication protocols that prioritize reliability and performance while operating in challenging underwater conditions. One key requirement is the ability to model complex network scenarios, including varying water depths, currents, and different network topologies. MATLAB’s built-in functions and toolboxes, such as the Communications System Toolbox, facilitate the simulation of underwater channels and signal processing techniques. This enables users to analyze the performance of various modulation schemes and error correction methods under realistic underwater conditions.

Additionally, MATLAB provides tools for implementing algorithms designed to address the unique challenges of underwater communication, such as high propagation delays and signal attenuation. These algorithms are critical for optimizing data transmission and reception in environments where conventional communication methods may not work effectively. By using MATLAB, developers can create and test these algorithms in a controlled environment before deploying them in real-world underwater applications.
Another significant requirement is data analysis capabilities. MATLAB excels at processing large datasets generated from underwater communication tests. Engineers can utilize its statistical and machine learning tools to analyze signal propagation, identify inefficiencies, and optimize resource usage, contributing to more robust and efficient communication systems.

This capability is essential for understanding how environmental factors, such as temperature, salinity, and pressure, affect communication performance.Lastly, MATLAB supports integration with hardware for real-time testing, allowing for the validation.

5.2 CODE

```
clc
clear;
close all;
warning off all
Nr_Repetitions = 1000;%24;                % Number of Monte Carlo repetitions
Mr_SNR_dB_OFDM = -5:5:30;                 % Signal-to-noise ratio
PerfectChannel_Knowledge = false;         % Perfect channel information or estimation
ModulationOrder = 4;                      % Modulation order, 4,16,64,...
LS = 12;                                  % Number of subcarriers
KL = 2^5;                                 % Number of symbols per Block = Spreading Length
Kall = KL*3+3;                            % Total Number of symbols (3 guard symbols!)
LTESubcarrierSpacing = 15e3;              % Subcarrier spacing (15kHz, same as LTE)
SamplingRate =  LTESubcarrierSpacing*LS*KL/4;  % Sampling rate (must be larger than
the subcarrier spacing times L)
%% OFDM Object
OFDM = OFDM(...
   LS,...                                 % Number of subcarriers
   KL/2*3,...                             % Number of OFDM Symbols
   LTESubcarrierSpacing,...               % Subcarrier spacing (Hz)
   SamplingRate,...                       % Sampling rate (Samples/s)
   0,...                                  % Intermediate frequency first subcarrier (Hz)
   false,...                              % Transmit real valued signal
   1/(LTESubcarrierSpacing*KL),   ...     % Cyclic prefix length (s)
1/SubcarrierSpacing/(K/2-1)
   (8-1/2)*1/LTESubcarrierSpacing*1/2 ...   % Zero guard length (s)
%% Alamouti Object
Alamouti = SpaceCoding(...
   'Alamouti2x1',...                      % Space time coding method
   1 ...                                  % Frequency spreading = 0; time spreading = 1 );
%% Modulation Object
```

```
Mod_Objecct = SignalConstellation(ModulationOrder,'CPM');
% For ML Detection
ML_MapIndex1 =
reshape(repmat((1:Mod_Objecct.ModulationOrder),Mod_Objecct.ModulationOrder,1),1,
Mod_Objecct.ModulationOrder^2);
ML_MapIndex2 =
reshape(repmat((1:Mod_Objecct.ModulationOrder).',1,Mod_Objecct.ModulationOrder),1
,Mod_Objecct.ModulationOrder^2);
ML_Mapping = Mod_Objecct.SymbolMapping([ML_MapIndex1;ML_MapIndex2]);
%% Pilot Matrix: 0=DataSymbol, 1=PilotSymbol, -1=ZeroSymbol;
PilotMatrixBlock_Antenna1 = zeros(LS,KL/2);
PilotMatrixBlock_Antenna1(2:6:end,1:8:end)=1;
PilotMatrixBlock_Antenna1(5:6:end,5:8:end)=1;
PilotMatrixBlock_Antenna1(2:6:end,2:8:end)=-1;
PilotMatrixBlock_Antenna1(5:6:end,6:8:end)=-1;
PilotMatrixBlock_Antenna2 = PilotMatrixBlock_Antenna1*(-1);
PilotMatrixBlock_Antenna(:,:,1) = PilotMatrixBlock_Antenna1;
PilotMatrixBlock_Antenna(:,:,2) = PilotMatrixBlock_Antenna2;
Nr_Pilots = sum(PilotMatrixBlock_Antenna1(:)==1);
Nr_DataSymbols = sum(PilotMatrixBlock_Antenna1(:)==0);
NrTransmittedSymbols = length(PilotMatrixBlock_Antenna1(:));
%% Channel Estimation Objects
ChannelEstimation_OFDM = PilotSymbolAidedChannelEstimation(...
   'Diamond',...                    % Pilot pattern
   [...                             % Matrix that represents the pilot pattern parameters
   LS,...              % Number of subcarriers
   6; ...                           % Pilot spacing in the frequency domain
   KL/2*3,...              % Number of OFDM Symbols
   4 ...                            % Pilot spacing in the time domain
   ],...
'linear'...                                    % Interpolation(Extrapolation) method
```

```
'linear','spline','FullAverage,'MovingBlockAverage'
   );
%-----------------------------------------------%
tic;
%% Simulate Over Different Channel Realizations
for i_rep = 1:100:Nr_Repetitions

%% Generate Data and Pilots
% Pilot Symbols: The pilot symbol power is by a factor of two higher because (pilots for the other antenna) are zero!
x_Pilot_Antenna1 = Mod_Objecct.SymbolMapping(randi(Mod_Objecct.ModulationOrder,Nr_Pilots,1));
x_Pilot_Antenna2 = Mod_Objecct.SymbolMapping(randi(Mod_Objecct.ModulationOrder,Nr_Pilots,1));
x_Pilot_Antenna1 = x_Pilot_Antenna1./abs(x_Pilot_Antenna1)*sqrt(2);
x_Pilot_Antenna2 = x_Pilot_Antenna2./abs(x_Pilot_Antenna2)*sqrt(2);

% Binary Data Stream
BinaryDataStream_Alamouti = randi([0 1],Nr_DataSymbols*log2(Mod_Objecct.ModulationOrder),1);
BinaryDataStream_SMAntenna1 = randi([0 1],Nr_DataSymbols*log2(Mod_Objecct.ModulationOrder),1); %Spatial Multiplexing
BinaryDataStream_SMAntenna2 = randi([0 1],Nr_DataSymbols*log2(Mod_Objecct.ModulationOrder),1); %Spatial Multiplexing

x_Alamouti = nan(LS,KL/2);
x_Alamouti(PilotMatrixBlock_Antenna1==0) = Mod_Objecct.Bit2Symbol(BinaryDataStream_Alamouti);
x_Alamouti_Coded = Alamouti.Encoder(x_Alamouti);
x_Alamouti_Coded(PilotMatrixBlock_Antenna==1)=[x_Pilot_Antenna1;x_Pilot_Antenna2];
x_Alamouti_Coded(PilotMatrixBlock_Antenna==-1)=0;
x_Alamouti_Coded_Antenna1 = x_Alamouti_Coded(:,:,1);
```

```
x_Alamouti_Coded_Antenna2 = x_Alamouti_Coded(:,:,2);
x_SM_Antenna1 = nan(LS,KL/2);
x_SM_Antenna1(PilotMatrixBlock_Antenna1==0) =
Mod_Objecct.Bit2Symbol(BinaryDataStream_SMAntenna1);
x_SM_Antenna1(PilotMatrixBlock_Antenna1==1) = x_Pilot_Antenna1;
x_SM_Antenna1(PilotMatrixBlock_Antenna1==-1) = 0;
x_SM_Antenna2 = nan(LS,KL/2);
x_SM_Antenna2(PilotMatrixBlock_Antenna2==0) =
Mod_Objecct.Bit2Symbol(BinaryDataStream_SMAntenna2);
x_SM_Antenna2(PilotMatrixBlock_Antenna2==1) = x_Pilot_Antenna2;
x_SM_Antenna2(PilotMatrixBlock_Antenna2==-1) = 0;

% Data symbols of the the first and second block (chosen randomly to keep it simple)
x_Block1_Antenna1 =
Mod_Objecct.SymbolMapping(randi(Mod_Objecct.ModulationOrder,LS,KL/2,1));
x_Block1_Antenna2 =
Mod_Objecct.SymbolMapping(randi(Mod_Objecct.ModulationOrder,LS,KL/2,1));
x_Block2_Antenna1 =
Mod_Objecct.SymbolMapping(randi(Mod_Objecct.ModulationOrder,LS,KL/2,1));
x_Block2_Antenna2 =
Mod_Objecct.SymbolMapping(randi(Mod_Objecct.ModulationOrder,LS,KL/2,1));

% Account for pilots in block 1 and 3
x_Block1_Antenna1(PilotMatrixBlock_Antenna1==1) =
x_Block1_Antenna1(PilotMatrixBlock_Antenna1==1)./abs(x_Block1_Antenna1(PilotMa
trixBlock_Antenna1==1))*sqrt(2);
x_Block1_Antenna2(PilotMatrixBlock_Antenna2==1) =
x_Block1_Antenna2(PilotMatrixBlock_Antenna2==1)./abs(x_Block1_Antenna2(PilotMa
trixBlock_Antenna2==1))*sqrt(2);
x_Block1_Antenna1(PilotMatrixBlock_Antenna1==-1) = 0;
x_Block1_Antenna2(PilotMatrixBlock_Antenna2==-1) = 0;
x_Block2_Antenna1(PilotMatrixBlock_Antenna1==1) =
```

```
x_Block2_Antenna1(PilotMatrixBlock_Antenna1==1)./abs(x_Block2_Antenna1(PilotMa
trixBlock_Antenna1==1))*sqrt(2);
x_Block2_Antenna2(PilotMatrixBlock_Antenna2==1) =
x_Block2_Antenna2(PilotMatrixBlock_Antenna2==1)./abs(x_Block2_Antenna2(PilotMa
trixBlock_Antenna2==1))*sqrt(2);
x_Block2_Antenna1(PilotMatrixBlock_Antenna1==-1) = 0;
x_Block2_Antenna2(PilotMatrixBlock_Antenna2==-1) = 0;

%% Transmitted Signal
TransmittedSymbols_OFDM_Alamouti_Antenna1 = [x_Block1_Antenna1
x_Alamouti_Coded_Antenna1 x_Block2_Antenna1];
TransmittedSymbols_OFDM_Alamouti_Antenna2 = [x_Block1_Antenna2
x_Alamouti_Coded_Antenna2 x_Block2_Antenna2];
s_OFDM_Alamouti_Antenna1 =
1/sqrt(2)*OFDM.Modulation(TransmittedSymbols_OFDM_Alamouti_Antenna1);
s_OFDM_Alamouti_Antenna2 =
1/sqrt(2)*OFDM.Modulation(TransmittedSymbols_OFDM_Alamouti_Antenna2);
TransmittedSymbols_OFDM_SM_Antenna1 = [x_Block1_Antenna1 x_SM_Antenna1
x_Block2_Antenna1];
TransmittedSymbols_OFDM_SM_Antenna2 = [x_Block1_Antenna2 x_SM_Antenna2
x_Block2_Antenna2];
s_OFDM_SM_Antenna1 =
1/sqrt(2)*OFDM.Modulation(TransmittedSymbols_OFDM_SM_Antenna1);
s_OFDM_SM_Antenna2 =
1/sqrt(2)*OFDM.Modulation(TransmittedSymbols_OFDM_SM_Antenna2);
%% Visible Light Channel
phi = 6;%irradiant angle
space = 2.5;%space between lights
phi =(phi/180 * pi);
%----------------------ENTER PARAMETERS-----------------------%
% Distance between tx and rx ( Meter )
heightLED = 1.48;
```

```
% Speed of Light
c = 300E6;
% Time
t = 0:0.01:4;
% Radius of light cone
radius = heightLED * tan(phi);
%----------------------END OF PARAMETERS-----------------------%
%%%%%%%%%%%%%%%%%%% Meshgrid X-axis and Y-axis %%%%%%%%%%%%%%%%
% Incidence angles of receiver according to X-Y axis %
[X,Y] = meshgrid(-4:0.2:4);
xydist = sqrt((X-space).^2 + (Y-space).^2);
hdist = sqrt(xydist.^2 + heightLED.^2);
incidence = atand(xydist.* heightLED ^(-1));
%%%%%%%%%%%%%%%%%%%%EndMesh%%%%%%%%%%%%%%%%%%%%%%
figure(1);hold on
[X1,Y1]=circle([space/2,space/2],radius,150);
plot(X1,Y1,'+')
% axis([-4 4 -4 4])
xlabel('Length of surface [m]')
ylabel('Breadth of surface [m]')
title('Top View of LEDs');hold on
[X1,Y1]=circle([space/2,-space/2],radius,150);
plot(X1,Y1,'+')
hold on
[X1,Y1]=circle([-space/2,space/2],radius,150);
plot(X1,Y1,'+')
hold on
[X1,Y1]=circle([-space/2,-space/2],radius,150);
plot(X1,Y1,'+')
%%%%%%%%%%%%%%%%% Received Power P1 2 3 4 in mW at each X-Y
```

```
location%%%%%%
%%%%%%%%%%%P1
[P, ~, Z, ~, ~, ~, ~]=RxSNR(incidence,hdist,t,phi); % SNR in dB at each X-Y location %
P1=P;
Z1=Z;
xydist = sqrt((X+space).^2 + (Y+space).^2);
hdist = sqrt(xydist.^2 + heightLED.^2);
incidence = atand(xydist.* heightLED ^(-1));
%%%%%%%%%%P2
[P, ~, Z, ~, ~, ~, ~]=RxSNR(incidence,hdist,t,phi); % SNR in dB at each X-Y location %
P2=P;
Z2=Z;
%%%%%%%%%%P3
xydist = sqrt((X-space).^2 + (Y+space).^2);
hdist = sqrt(xydist.^2 + heightLED.^2);
incidence = atand(xydist.* heightLED ^(-1));
[P, ~, Z, ~, ~, ~, ~]=RxSNR(incidence,hdist,t,phi); % SNR in dB at each X-Y location %
P3=P;
Z3=Z;
%%%%%%%%%%P4
xydist = sqrt((X+space).^2 + (Y-space).^2);
hdist = sqrt(xydist.^2 + heightLED.^2);
incidence = atand(xydist.* heightLED ^(-1));
[P, PO, Z, impulset, impulsetd, impulsef, impulsefd]=RxSNR(incidence,hdist,t,phi); %
SNR in dB at each X-Y location %
P4=P;
Z4=Z;
%%%%%%%%%%P TOTAL
P=P1+P2+P3+P4;
Z=Z1+Z2+Z3+Z4;
%%%%%%%%%%%%%%%%%%%%%%%%%END RxSNR TOTAL RECEIVED
```

```
POWER%%%%%%%%%%%%%%%%%%%%%%%%%%
%%%%%%%%%%%%%%%%%%%%%%%%%%%PLot 3D diagram for DATARATE %%%%%%%%%%%%%%%%%%%%%%%%%%
C= 50*10^6*log2(1+Z);
figure(2);
[X1,Y1] = meshgrid(-5:0.25:5);
surf(X1,Y1,C)
colormap(hsv);
shading interp
xlabel('Length of room [m]')
ylabel('Width of room [m]')
zlabel('Datarate in (bits/sec)')
title('DataRate Distribution')
hold off

%%%%%%%%%%%%%%%%%%%%%Plot 3D diagram for Received Power%%%%%%%%%%%%%%%%%
figure(3);
surf(X,Y,P)
colormap(hsv);
shading interp
axis([-5 5 -5 5 0 1.5e-4])
xlabel('Length of room [m]')
ylabel('Width of room [m]')
zlabel('Received Power in (W)')
title('Receivered Power Distribution')
hold off
R_space = 0.5;
xlocation =0.7;
ylocation =0.5;
% underwater channel propagation
signal=[real(s_OFDM_SM_Antenna1) real(s_OFDM_SM_Antenna2)];
```

```
% UnderwaterOC_propagation(signal)

%%%%%%%%%%%%%%%%%%%%%%%%%%%% GAIN VALUE
%%%%%%%%%%%%%%%%%%%%%%%%%%%%%%%%%%%%%%%%%%%%
h11=channelgain(xlocation-R_space-space,ylocation+R_space+space,phi,space);
h12=channelgain(xlocation+R_space-space,ylocation+R_space+space,phi,space);
h13=channelgain(xlocation+R_space-space,ylocation-R_space+space,phi,space);
h14=channelgain(xlocation-R_space-space,ylocation-R_space+space,phi,space);
h21=channelgain(xlocation-R_space+space,ylocation+R_space+space,phi,space);
h22=channelgain(xlocation+R_space+space,ylocation+R_space+space,phi,space);
h23=channelgain(xlocation+R_space+space,ylocation-R_space+space,phi,space);
h24=channelgain(xlocation-R_space+space,ylocation-R_space+space,phi,space);
h31=channelgain(xlocation-R_space+space,ylocation+R_space-space,phi,space);
h32=channelgain(xlocation+R_space+space,ylocation+R_space-space,phi,space);
h33=channelgain(xlocation+R_space+space,ylocation-R_space-space,phi,space);
h34=channelgain(xlocation-R_space+space,ylocation-R_space-space,phi,space);
h41=channelgain(xlocation-R_space-space,ylocation+R_space-space,phi,space);
h42=channelgain(xlocation+R_space-space,ylocation+R_space-space,phi,space);
h43=channelgain(xlocation+R_space-space,ylocation-R_space-space,phi,space);
h44=channelgain(xlocation-R_space-space,ylocation-R_space-space,phi,space);
%%%%%%%%%%%%%%%%%%%%%%%%%%%% END GAIN VALUE
%%%%%%%%%%%%%%%%%%%%%%%%%%%%%%%%%%%%%%%%%%%%
h=[h11,h12,h13,h14;h11,h22,h23,h24;h31,h32,h33,h34;h41,h42,h43,h44];
figure(4);
subplot(211);surf(h)
colormap(jet);
shading interp
xlabel('Number of Transmit antenna')
ylabel('Number of Receive antenna')
zlabel('Channel Gain matrix')
title('VLC channel Gain matrix')
hold off
```

```
subplot(212);
bar(reshape(h,1,16));
xlabel('Time(s)')
ylabel('Normalized Intensity')
title('Impulse response of fading channel')

%%%%%%%%%%%%%%%%%%%%%%%%%%%%%%%%%%%%%%%%%%%%%
%%%%%%%%%%%%%%%%%%%%%%%%%%%%%%
Ptx =0.1;
Prx = Ptx * h;
% (supportet by our measurements for a small number of subcarriers and multicarrier
symbols)
h11 = sqrt(1/2)*(randn+1j*randn)*mean(Prx(1,:))*0.2e6;
h12 = sqrt(1/2)*(randn+1j*randn)*mean(Prx(1,:))*0.2e6;
h21 = sqrt(1/2)*(randn+1j*randn)*mean(Prx(1,:))*0.2e6;
h22 = sqrt(1/2)*(randn+1j*randn)*mean(Prx(1,:))*0.2e6;
powerPbit=length(Mr_SNR_dB_OFDM);
%% Receiver Part
for i_S = 1:powerPbit
SNR_dB_OFDM = Mr_SNR_dB_OFDM(i_S);
Pn = SamplingRate/(LTESubcarrierSpacing*LS)*10^(-SNR_dB_OFDM/10);
noise_Antenna1 =
sqrt(Pn/2)*(randn(size(s_OFDM_Alamouti_Antenna1))+1j*randn(size(s_OFDM_Alamo
uti_Antenna1)));
noise_Antenna2 =
sqrt(Pn/2)*(randn(size(s_OFDM_Alamouti_Antenna1))+1j*randn(size(s_OFDM_Alamo
uti_Antenna1)));

%% Received Signal
r_OFDM_Alamouti_Antenna1 =
h11*s_OFDM_Alamouti_Antenna1+h12*s_OFDM_Alamouti_Antenna2+noise_Antenna
r_OFDM_SM_Antenna1
```

```
=h11*s_OFDM_SM_Antenna1+h12*s_OFDM_SM_Antenna2+noise_Antenna1;
r_OFDM_SM_Antenna2
=h21*s_OFDM_SM_Antenna1+h22*s_OFDM_SM_Antenna2+noise_Antenna2;

%% demodulation
 y_OFDM_Alamouti_3Blocks = OFDM.Demodulation(r_OFDM_Alamouti_Antenna1);
y_OFDM_Alamouti = y_OFDM_Alamouti_3Blocks(:,(1:KL/2)+KL/2);
 y_OFDM_SM_Antenna1_3Blocks = OFDM.Demodulation(r_OFDM_SM_Antenna1);
y_OFDM_SM_Antenna1 = y_OFDM_SM_Antenna1_3Blocks(:,(1:KL/2)+KL/2);
y_OFDM_SM_Antenna2_3Blocks = OFDM.Demodulation(r_OFDM_SM_Antenna2);
y_OFDM_SM_Antenna2 = y_OFDM_SM_Antenna2_3Blocks(:,(1:KL/2)+KL/2);
%% Noise and Power Estimation
noise_OFDM_Antenna1_3Blocks = OFDM.Demodulation(noise_Antenna1);
noise_OFDM_Antenna1 = noise_OFDM_Antenna1_3Blocks(:,(1:KL/2)+KL/2);
noise_OFDM_Antenna2_3Blocks = OFDM.Demodulation(noise_Antenna2);
noise_OFDM_Antenna2 = noise_OFDM_Antenna2_3Blocks(:,(1:KL/2)+KL/2);
Pn_OFDM_Antenna1(i_S,i_rep) = mean(abs(noise_OFDM_Antenna1(:)).^2);
Pn_OFDM_Antenna2(i_S,i_rep) = mean(abs(noise_OFDM_Antenna2(:)).^2);
PSignalPlusNoise_OFDM_Alamouti(i_S,i_rep) = mean(abs(y_OFDM_Alamouti(:)).^2);
PSignalPlusNoise_OFDM_SM_Antenna1(i_S,i_rep)                                    =
mean(abs(y_OFDM_SM_Antenna1(:)).^2);
PSignalPlusNoise_OFDM_SM_Antenna2(i_S,i_rep)                                    =
mean(abs(y_OFDM_SM_Antenna2(:)).^2);

%% Channel Estimation
EstimatedChannel_OFDM_Alamouti(:,:,1)                                           =
mean(y_OFDM_Alamouti(PilotMatrixBlock_Antenna1==1)./x_Pilot_Antenna1)*ones(L
S,KL/2);
EstimatedChannel_OFDM_Alamouti(:,:,2)                                           =
mean(y_OFDM_Alamouti(PilotMatrixBlock_Antenna2==1)./x_Pilot_Antenna2)*ones(L
S,KL/2);
% OFDM  :  PowerNormalization (Note that the noise power is also increasd=> The same
```

```
SNR (ignoring zero guard))
H11_Est_OFDM =
mean(y_OFDM_SM_Antenna1(PilotMatrixBlock_Antenna1==1)./x_Pilot_Antenna1);
H21_Est_OFDM =
mean(y_OFDM_SM_Antenna2(PilotMatrixBlock_Antenna1==1)./x_Pilot_Antenna1);
H12_Est_OFDM =
mean(y_OFDM_SM_Antenna1(PilotMatrixBlock_Antenna2==1)./x_Pilot_Antenna2);
H22_Est_OFDM =
mean(y_OFDM_SM_Antenna2(PilotMatrixBlock_Antenna2==1)./x_Pilot_Antenna2);
if PerfectChannel_Knowledge
   % The power is split between TX Antennta 1 and 2, which shows in the channel
   EstimatedChannel_OFDM_Alamouti(:,:,1) = h11/sqrt(2)*ones(LS,KL/2);
   EstimatedChannel_OFDM_Alamouti(:,:,2) = h12/sqrt(2)*ones(LS,KL/2);

   H11_Est_OFDM = h11/sqrt(2);
   H21_Est_OFDM = h21/sqrt(2);
   H12_Est_OFDM = h12/sqrt(2);
   H22_Est_OFDM = h22/sqrt(2);
end
H_Est_OFDM =[H11_Est_OFDM,H12_Est_OFDM;H21_Est_OFDM,H22_Est_OFDM];
%% Data Detection
%Estimated Symbols
x_est_OFDM_Alamouti =
Alamouti.Decoder(y_OFDM_Alamouti,EstimatedChannel_OFDM_Alamouti*sqrt(2));
% ML Detection
y_OFDM_SM_Temp =
repmat(reshape([y_OFDM_SM_Antenna1(:).';y_OFDM_SM_Antenna2(:).'],2,1,[]),1,Mo
d_Objecct.ModulationOrder^2);
[~,indexMin] = min(sum(abs(y_OFDM_SM_Temp-
reshape(repmat(H_Est_OFDM*ML_Mapping,1,LS*KL/2),size(y_OFDM_SM_Temp))).
^2),[],2);
x_est_OFDM_SM_ML = reshape(ML_Mapping(:,indexMin(:)).',LS,KL/2,2);
```

```
% Symbols To Bit
DetectedBitStream_OFDM_Alamouti =
Mod_Objecct.Symbol2Bit(x_est_OFDM_Alamouti(PilotMatrixBlock_Antenna1==0));
DetectedBitStream_OFDM_SM_ML =
Mod_Objecct.Symbol2Bit(x_est_OFDM_SM_ML(PilotMatrixBlock_Antenna==0));

% Bit Error Ratio
BER_OFDM_Alamouti(i_S,i_rep) =
mean(BinaryDataStream_Alamouti~=DetectedBitStream_OFDM_Alamouti);
BER_OFDM_SM_ML(i_S,i_rep) =
mean([BinaryDataStream_SMAntenna1;BinaryDataStream_SMAntenna2]~=DetectedBit
Stream_OFDM_SM_ML);
end

TimePassed = toc;
if mod(i_rep,100)==0
disp(['Realization ' int2str(i_rep) ' of ' int2str(Nr_Repetitions) '. Time left: '
int2str(TimePassed/i_rep*(Nr_Repetitions-i_rep)/60) 'minutes']);
end
end
UnderwaterOC_propagation(signal);

%figure();
%ChannelEstimation_OFDM.PlotPilotPattern;
%title('Symbols of MIMO');

[Power_OFDM,~] = OFDM.PlotTransmitPower;
%figure();
%plot(t_OFDM,Power_OFDM,'b-s','linewidth',2);
%ylabel('Transmit Power');
%xlabel('Time(s)');
%title('SM-MIMO signal transmission power');
%% Calculate Power Spectral Density
```

```
[PSD_OFDM,t_OFDM] = OFDM.PlotPowerSpectralDensity;
%figure();
%plot(t_OFDM,fftshift(10*log10((PSD_OFDM))),'red ');
%ylabel('Power Spectral Density (dB)');
%xlabel('Frequency (Hz)');
%title('Spectrum of UWOC signal');
Disin=Mr_SNR_dB_OFDM;
load Paper_result
figure();
semilogy(Disin,mean(BER_OFDM_SM_ML,2),'-s black','linewidth',2);
hold on;
semilogy(Disin,mean(BER_OFDM_Alamouti,2),'-o green','linewidth',2);
hold on;
semilogy(Disin,D1,'-s red','linewidth',2);
hold on;
semilogy(Disin,D2,'-o blue','linewidth',2);
grid on;
legend('MIMO 2x2 with EGC-CPM','MIMO 2x2 with OC-CPM','MIMO 2x2 with EGC-
OOK',...
   'MIMO 2x2 with OC-OOK','location','best');
xlabel('Average transmitted power per bit[dBm]');
ylabel('Bit Error Ratio');
title('BER of 25 m coastal water link');
figure;semilogy(Mr_SNR_dB_OFDM,BER_OFDM_SM_ML(:,1:100:500),'-
d','linewidth',2);
grid on;
legend('MIMO 2x2-Sim','MISO 2x1-Sim','SISO-Analytic','MIMO 2x2-Analytic','MISO
2x1-Analytic','location','best');
xlabel('Average transmitted power per bit[dBm]');
ylabel('Bit Error Ratio');
title('BER of 25 m coastal water link with \sigma_x=0.1');
```

```
figure;semilogy(Mr_SNR_dB_OFDM,BER_OFDM_SM_ML(:,501:100:end),'-
p','linewidth',2);
grid on;
legend('MIMO 2x2-Sim','MISO 2x1-Sim','SISO-Analytic','MIMO 2x2-Analytic','MISO
2x1-Analytic','location','best');
xlabel('Average transmitted power per bit[dBm]');
ylabel('Bit Error Ratio');
title('BER of 25 m coastal water link with \sigma_x=0.4');
figure;semilogy(Mr_SNR_dB_OFDM,BER_OFDM_Alamouti(:,1:100:500),'-
d','linewidth',2);
grid on;
legend('MIMO 2x2','MISO 2x1','SISO','MISO 3x1','SIMO 1x2','location','best');
xlabel('Average transmitted power per bit[dBm]');
ylabel('Bit Error Ratio');
title('BER of 25 m coastal water link with R_b=0.5Gbps');
figure;semilogy(Mr_SNR_dB_OFDM,BER_OFDM_Alamouti(:,501:100:end),'-
p','linewidth',2);
grid on;
legend('MISO 2x1','MISO 3x1','MIMO 2x2','SISO','SIMO 1x2','location','best');
xlabel('Average transmitted power per bit[dBm]');
ylabel('Bit Error Ratio');
title('BER of 25 m coastal water link with R_b=50Gbps');
```

CHAPTER 6

RESULTS ANALYSIS AND REPORT

6.1RESULTS

The figure presents a top view of LEDs positioned at the four corners of a rectangular surface, with each LED represented by colored circular markers, possibly indicating their positions and signal characteristics. The axes denote the length and breadth of the surface in meters, suggesting a spatial layout for analysis.

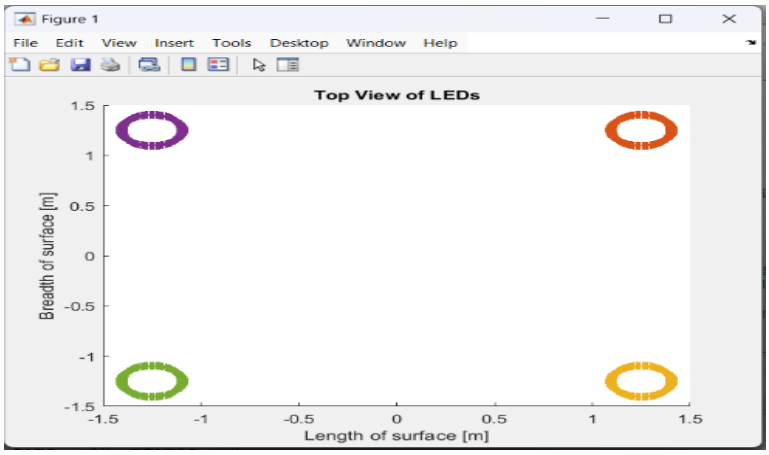

Figure 6.1 Top View of LEDs

The figure illustrates the data rate distribution in a room using a 3D surface plot, where different colors represent variations in data rate values. The axes indicate the room's width and length in meters, while the vertical axis represents the data rate in bits per second.

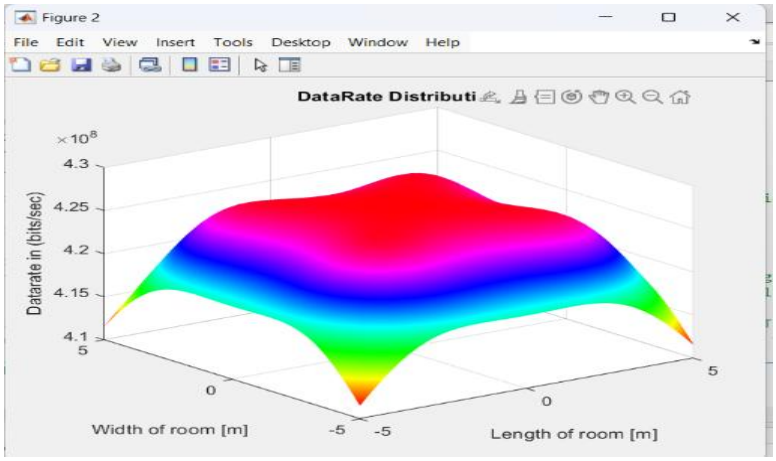

Figure 6.2 Rainbow effect of Data Distribution

The figure illustrates the data rate distribution in a room using a 3D surface plot, where different colors represent variations in data rate values. The axes indicate the room's width and length in meters, while the vertical axis represents the data rate in bits per second. The plot shows a peak in the center, suggesting higher data rates in that region and lower values near the edges.

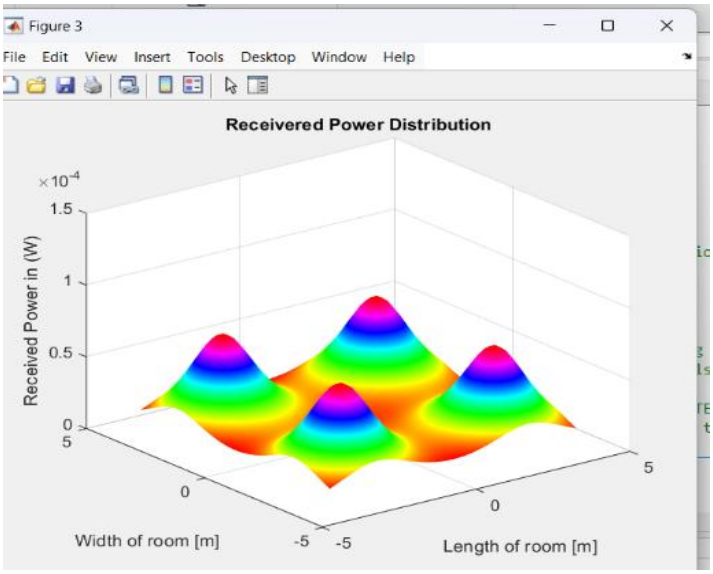

Figure 6.3 Received power Distribution

The figure depicts the received power distribution in a room using a 3D surface plot, where different colors indicate variations in power levels. The axes represent the room's width and length in meters, while the vertical axis shows the received power in nanowatts.

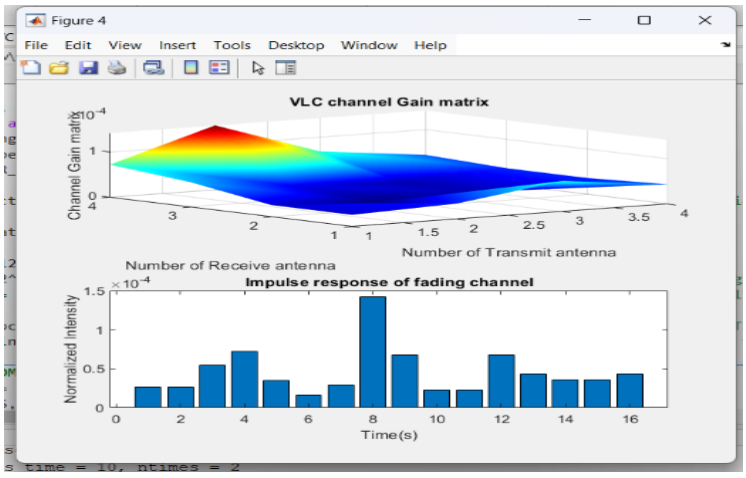

Figure 6.4 VLC channel gain Matrix

The figure presents two subplots related to Visible Light Communication (VLC). The top plot shows the channel gain matrix, illustrating the relationship between the number of transmit and receive antennas. The bottom plot depicts the impulse response of a fading channel, indicating variations in signal intensity over time due to multipath effects. The variations in amplitude and dispersion in the output signal suggest the impact of underwater channel impairments such as attenuation, multipath propagation, and Doppler effects. The noise and signal degradation observed in the lower plot highlight the challenges in maintaining signal integrity in underwater environments.

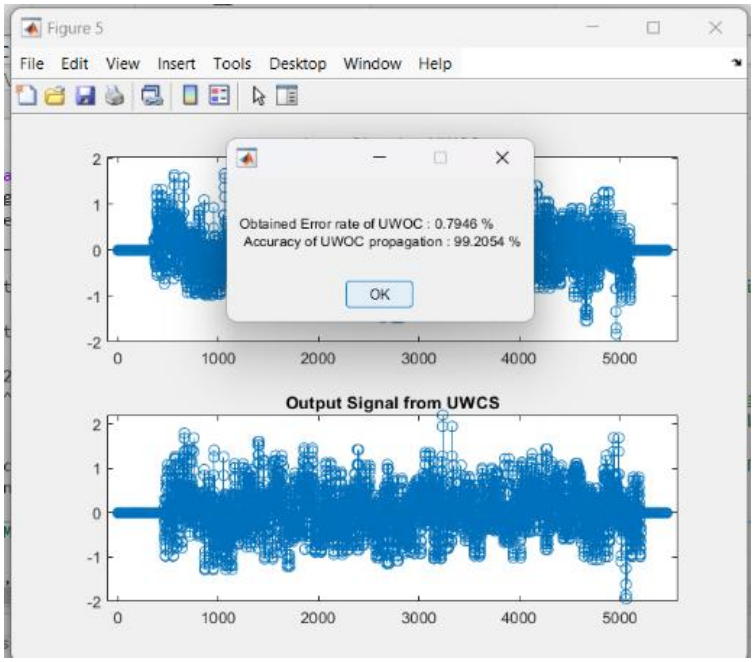

Figure 6.5 Accuracy of UWC Propagation

The variations in amplitude and dispersion in the output signal suggest the impact of underwater channel impairments such as attenuation, multipath propagation, and Doppler effects. The noise and signal degradation observed in the lower plot highlight the challenges in maintaining signal integrity in underwater environments. Effective equalization and error correction techniques are crucial to mitigate these distortions and enhance communication reliability. This analysis helps in optimizing modulation and coding schemes for improved underwater wireless data transmission. The presence of noise and signal degradation, as observed in the lower signal plots, emphasizes the difficulty in preserving signal integrity in dynamic and harsh underwater environments.

Such distortions not only reduce the effective data rate but also increase the bit error rate, affecting the reliability of the communication link. To combat these issues, robust equalization techniques—which compensate for channel-induced distortions—and error correction codes, such as convolutional or turbo codes, are essential. These methods help recover the original data despite the impairments introduced during propagation.

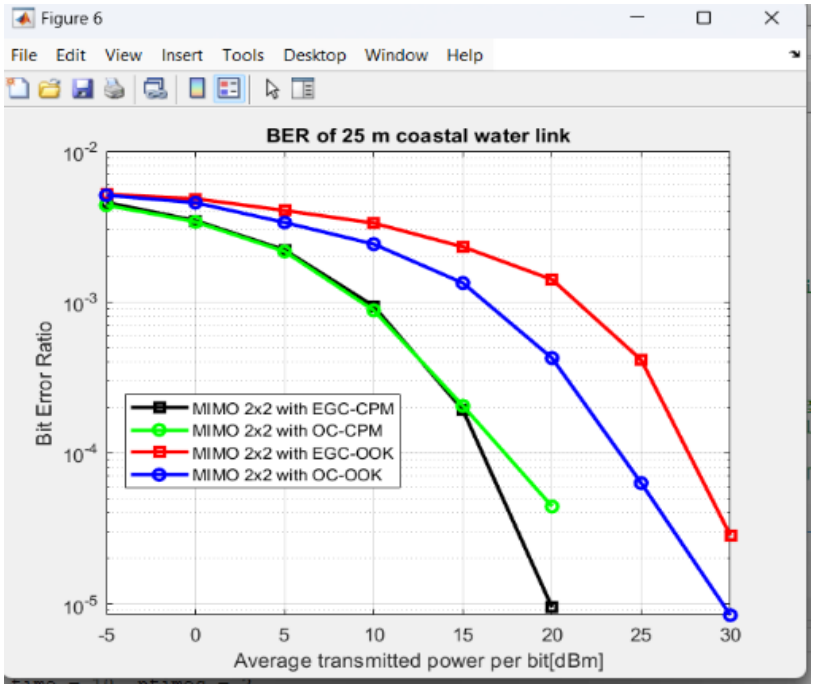

Figure 6.6 Bit Error Ratio of 25m

6.2 ADVANTAGES

1. Understanding Current Trends

Surveys help identify the latest advancements, challenges, and technologies in underwater wireless communication, such as acoustic, radio frequency (RF), and optical communication.

2. Identifying Challenges and Gaps

Underwater communication faces issues like high attenuation, limited bandwidth, multipath effects, and long propagation delays. Surveys highlight these challenges and suggest possible solutions.

3.Comparing Different Technologies

A structured survey helps compare different UWC techniques (acoustic, RF, and optical) based on parameters like range, data rate, power consumption, and environmental impact.

4.Enhancing Future Research and Development

By analyzing existing studies, researchers can identify areas needing further investigation, leading to innovations in modulation techniques, networking protocols, and energy-efficient systems.

6.Economic and Environmental Impact Assessment

Understanding cost-effective and eco-friendly UWC solutions is crucial for sustainable ocean monitoring and resource management.

7.Supporting Marine and Defense Applications

UWC is vital for applications like underwater exploration, naval defense, oceanographic data collection, and submarine communication. A survey can guide the selection of appropriate technologies for these fields.

6.3 APPLICATIONS

1. Marine and Oceanographic Research

Underwater communication technology is essential for real-time ocean monitoring and scientific exploration. It enables researchers to collect data on temperature, salinity, currents, and marine biodiversity through underwater sensor networks. These insights help in studying climate change, ocean circulation, and marine ecosystems.

2. Defense and Naval Communication

Military and defense operations rely on secure underwater communication for submarine-to-submarine and submarine-to-surface interactions. UWC technology enables covert communication, underwater surveillance, and mine detection, enhancing national security and naval strategies.

3. Underwater Exploration and Archaeology

Underwater communication supports deep-sea exploration and the study of submerged historical sites such as shipwrecks and ancient underwater cities. It allows remotely operated vehicles (ROVs) to transmit data in real time, assisting researchers in documenting and preserving underwater artifacts.

4. Disaster Monitoring and Mitigation

Underwater sensor networks are vital for disaster prediction and response. They play a key role in tsunami and earthquake early warning systems, enabling real-time alerts. Additionally, they assist in search-and-rescue operations by providing crucial communication links in disaster-affected underwater regions.

5. Water Pollution Monitoring

UWC technology is widely used to monitor oil spills, plastic waste, and chemical pollution in oceans, rivers, and lakes. Real-time data from underwater sensors helps authorities take quick action to mitigate environmental hazards, ensuring cleaner and healthier aquatic ecosystems.

CHAPTER 7

CONCLUSION AND FUTURE SCOPE

7.1 CONCLUSION

Underwater wireless communication (UWC) is a rapidly evolving field with significant implications for scientific research, military defense, industrial applications, and environmental monitoring. The survey of UWC technology provides a comprehensive understanding of various communication techniques, including acoustic, optical, and radio frequency (RF) signals, each with its own advantages and limitations based on factors such as propagation range, bandwidth, energy consumption, and environmental impact. Acoustic communication, being the most commonly used method, offers long-range transmission capabilities but suffers from high latency and limited bandwidth. Optical communication provides higher data rates but is highly susceptible to absorption and scattering in water, making it effective only for short distances in clear water. Meanwhile, RF communication, despite its potential for higher data transfer rates, is significantly hindered by the high conductivity of seawater, limiting its practical applications.

These limitations emphasize the need for innovative solutions, such as hybrid communication models, advanced signal processing techniques, and adaptive networking protocols to enhance data transmission reliability and efficiency in underwater environments. The survey also highlights key challenges faced in UWC, including multipath interference, Doppler shift, energy efficiency constraints, and security vulnerabilities. Addressing these challenges requires the development of robust error correction mechanisms, power-efficient transceiver designs, and secure communication protocols to ensure seamless and reliable data transfer across underwater networks. Additionally, the increasing integration of artificial intelligence (AI) and machine learning (ML) into UWC systems is driving advancements in autonomous decision-making, predictive analytics, and real-time data processing, which are crucial for enhancing the performance of underwater sensor networks, remotely operated vehicles (ROVs), and autonomous underwater vehicles (AUVs). Furthermore, the Internet of Underwater Things (IoUT) is emerging as a transformative concept, enabling interconnected smart underwater devices to facilitate real-time monitoring, environmental conservation, and deep-sea

exploration. The survey underscores the significant role of UWC in various real-world applications, including oceanographic data collection, submarine communication, offshore oil and gas operations, disaster monitoring, and underwater surveillance. In oceanographic research, UWC enables continuous environmental monitoring, providing valuable data on ocean temperature, salinity, and marine biodiversity, which is essential for understanding climate change and ecosystem dynamics. In military and defense sectors, secure and covert underwater communication is crucial for naval operations, anti-submarine warfare, and underwater reconnaissance missions, where reliable and encrypted data transmission is paramount. Moreover, industries such as offshore oil and gas heavily rely on UWC for the real-time monitoring of underwater infrastructure, ensuring the safety and efficiency of deep-sea drilling and pipeline operations.

7.2 FUTURE SCOPE

The future of underwater wireless communication (UWC) is poised for significant advancements, driven by emerging technologies and increasing demand for reliable, high-speed, and energy-efficient underwater networks. As global interest in ocean exploration, environmental monitoring, and underwater surveillance grows, the development of more robust and scalable communication systems will be crucial. One of the most promising areas of future research is the enhancement of hybrid communication models, combining acoustic, optical, and radio frequency (RF) technologies to maximize efficiency and overcome the limitations of individual methods. Hybrid systems can enable high-speed data transmission over short distances using optical communication, while acoustic signals handle long-range data exchange and RF technology facilitates shallow-water and near-surface communication. Another key aspect of future development is the integration of Artificial Intelligence (AI) and Machine Learning (ML) into UWC networks. AI-driven algorithms can improve adaptive modulation, signal processing, and real-time decision-making, allowing underwater communication systems to dynamically adjust to environmental changes such as water turbulence, temperature variations, and signal interference.

Additionally, the emergence of the Internet of Underwater Things (IoUT) will revolutionize underwater communication by enabling a network of interconnected

underwater devices, including autonomous underwater vehicles (AUVs), remotely operated vehicles (ROVs), and smart sensor networks. These systems will facilitate real-time data collection, analysis, and sharing across multiple underwater platforms, significantly benefiting applications such as oceanographic research, military operations, deep-sea mining, and offshore infrastructure monitoring. Furthermore, advancements in energy-efficient underwater transceivers and self-powered communication nodes will address the current challenges of power consumption in underwater sensor networks. Research into wireless power transfer (WPT), energy harvesting technologies, and low-power electronics will enable longer operational lifetimes for underwater sensor networks without frequent battery replacements.

Another promising area is the development of next-generation modulation techniques, such as orthogonal frequency-division multiplexing (OFDM) and spread spectrum techniques, which can enhance bandwidth utilization and signal robustness in harsh underwater conditions. Additionally, efforts to standardize underwater communication protocols and frequency bands will promote better interoperability between different UWC systems used by various industries and research institutions worldwide. The adoption of 5G and beyond for underwater networks, along with advancements in quantum communication and underwater Li-Fi technology, may lead to unprecedented breakthroughs in high-speed underwater data transmission.

REFERENCES

[1]. Stojanovic, M. (2007) – "On the Relationship Between Capacity and Distance in an Underwater Acoustic Communication Channel." *IEEE Journal of Oceanic Engineering, 32(4), 985-996.*

[2]. Akyildiz, I. F., Pompili, D., & Melodia, T. (2005) – "Underwater Acoustic Sensor Networks: Research Challenges." *Ad Hoc Networks, 3(3), 257-279.*

[3]. Heidemann, J., Stojanovic, M., & Zorzi, M. (2012) – "Underwater Sensor Networks: Applications, Advances, and Challenges." *Philosophical Transactions of the Royal Society A: Mathematical, Physical and Engineering Sciences, 370(1958), 158-175.*

[4]. Xie, P., Zhou, Z., Peng, Z., & Cui, J. H. (2009) – "Link Layer Protocols for Underwater Acoustic Networks: A Survey." *Wireless Communications and Mobile Computing, 9(10), 1257-1273.*

[5]. Zorzi, M., & Melodia, T. (2006) – "A Cross-Layer Approach to MAC and Routing for Underwater Acoustic Sensor Networks." *Proceedings of IEEE/OES OCEANS Conference, Boston, MA.*

[6]. Chitre, M., Shahabudeen, S., & Stojanovic, M. (2008) – "Underwater Acoustic Communications and Networking: Recent Advances and Future Challenges." *Marine Technology Society Journal, 42(1), 103-116.*

[7]. Akyildiz, I. F., & Jornet, J. M. (2010) – "The Internet of Nano-Things." *IEEE Wireless Communications, 17(6), 58-63.*

[8].Domingo, M. C. (2011) – "Magnetic Induction for Underwater Wireless Communication Networks." *IEEE Transactions on Antennas and Propagation, 60(6).*

[9]. Sharma, V., & Saha, R. (2019) – "Comparative Study of Underwater Wireless Communication Techniques." *International Journal of Computer Applications*.

APPENDIX

This appendix provides additional information supporting the research and development of the Underwater Wireless Communication Technology project. It includes definitions of key acronyms, technical details of various communication methods, a summary of experimental setups, and relevant code and references.To clarify commonly used terms throughout the report, several acronyms are defined here. *UWC* stands for Underwater Wireless Communication, while *EM* refers to Electromagnetic Waves. *RF* is short for Radio Frequency, and *AUV* denotes Autonomous Underwater Vehicles. *SONAR* refers to Sound Navigation and Ranging, and *UWAC* represents Underwater Acoustic Communication. *UOWC* is an abbreviation for Underwater Optical Wireless Communication, and performance metrics such as *SNR* (Signal-to-Noise Ratio) and *BER* (Bit Error Rate) are also commonly referenced.

Three primary underwater wireless communication methods were explored in this project: acoustic, optical, and radio frequency communication. Acoustic communication, typically operating between 10 Hz and 1 MHz, can cover long distances up to 20 km but suffers from low data rates (generally under 100 kbps) and high latency due to the slow propagation of sound in water. It is, however, robust in turbid environments and widely used in deep-sea applications. Optical communication, using visible light frequencies (around 430–770 THz), offers high-speed data transfer up to 10 Gbps but has a limited range of less than 100 meters and is highly affected by water clarity and the need for line-of-sight. RF communication, though limited to ranges below 10 meters due to high attenuation in saltwater, may still be useful for short-range, low-latency applications in shallow waters.

In a controlled laboratory setting, a basic experimental setup was used to test underwater optical communication. A water tank measuring 5 meters by 2 meters by 2 meters was used to simulate underwater conditions. A blue-green LED served as the transmitter, while a photodiode equipped with an optical filter functioned as the receiver. Tests were conducted at various distances (1m, 5m, and 10m), and key performance metrics such as BER, SNR, and signal strength were recorded under varying turbidity conditions. Supporting diagrams were included in the main body.

These include a comparative chart of signal attenuation across different media, a schematic of the optical communication setup, and a data visualization showing data rate versus distance for various technologies.Additionally, a simple Python code snippet was developed to calculate the Signal-to-Noise Ratio (SNR) in an acoustic channel. The code takes input values for signal and noise power and calculates the SNR in decibels, aiding in the analysis and validation of experimental data.

Finally, the following references were consulted to guide the technical development of the project: Akyildiz et al. (2005) discussed the challenges in underwater acoustic sensor networks; Zeng et al. (2017) provided an extensive survey on underwater optical wireless communications; and relevant IEEE standards, such as IEEE P1902.1, offered frameworks for nanoscale and molecular communication.This appendix aims to consolidate essential background information, technical data, and resources to enhance the understanding and reproducibility of the project.